8-24-2022 9:30 AM

Conducting Polypyrrole Hydrogel Biomaterials For Drug Delivery And Cartilage Tissue Regeneration

Iryna Liubchak, *The University of Western Ontario*

Supervisor: Price, Aaron D., *The University of Western Ontario*

A thesis submitted in partial fulfillment of the requirements for the Master of Engineering Science degree in Biomedical Engineering

Abstract

Articular cartilage tissue has limited capacity for self-regeneration leading to challenges in the treatment of joint injuries and diseases such as osteoarthritis. The tissue engineering approach combines biomaterials, cells and bioactive molecules to provide a long-term and stable cartilage repair. In the following work, electroactive polymer polypyrrole (PPy) was incorporated into the synthetic hydrogel to enhance the mechanical properties of the material for cartilage applications. PPy was loaded with drug compound and the *on demand* drug release was demonstrated. The composite PPy hydrogel was 3D printed using stereolithography to create a porous tissue engineering scaffold. Biocompatibility and cell adhesion to the material were investigated to ensure their applicability in cartilage regenerative applications. Fabricated composite polymers were successful as potential biomaterials for cartilage tissue engineering scaffolds.

Keywords: cartilage regeneration, polypyrrole, drug delivery, hydrogels, electroactive polymers, 3D printing.

Summary for Lay Audience

Cartilage tissue repair presents a significant challenge for clinicians and scientists. In healthy joints, cartilage acts as a protective layer covering the bone surface and helps mitigate the high mechanical load joints in the human body are exposed to daily. When cartilage tissue breaks down due to inflammation or injury to the joint, the bone surface is left unprotected, leading to high pain levels, and a decrease in the range of motion ultimately leading to disability. Due to the absence of direct blood supply, cartilage has a very limited capacity for self-regeneration. Tissue engineering is a promising approach that can induce and support cartilage repair. It combines biomaterials providing structural replacement at the site of the defect, cells responsible for the formation of new tissue, and bioactive molecules that turn on or off certain cell activities or metabolic processes in the surrounding tissues. Hydrogel biomaterials have been recognized as being structurally similar to cartilage tissue, however, they have to be paired with a second polymer for improved functionality. Polypyrrole is a *smart* polymer that can store medicinal compounds and release them *on demand*, making it an attractive material for biomedical applications. Hydrogel/polypyrrole composite materials were produced in this study for potential use in cartilage tissue engineering. These materials were not toxic to cartilaginous cells and even supported their attachment to the surface. To ensure the functionality of the material, it was tested for drug delivery capabilities. Moreover, the porous hydrogel/polypyrrole structure was 3D printed and can be investigated for use in tissue engineering scaffolds.

Co-Authorship Statement

This MESc thesis has been prepared by Iryna Liubchak and reviewed by Dr. A. D. Price according to regulations of the School of Graduate and Postdoctoral Studies at Western University and has been co-authored as follows:

Chapter 3. ***PEGDA-PPy hydrogel fabrication***

All the experiments and data analysis were conducted by Iryna Liubchak under the supervision of Dr. A. D. Price. Experimental methodology for section 3.3.4 was designed in collaboration with F. Benjamin Holness and Dr. N. Lanigan.

Chapter 4. ***Drug delivery from PEGDA-PPy hydrogels***

All the experiments and data analysis were conducted by Iryna Liubchak under the supervision of Dr. A. D. Price.

Chapter 5. ***PEGDA-PPy biocompatibility***

All the experiments and data analysis were conducted by Iryna Liubchak under the supervision of Dr. C. Sèguin and Dr. A. D. Price. Experimental methodology was designed in collaboration with Dr. C. Sèguin, Courtney Brooks and Matthew Lawrence. The paper co-authored by Iryna Liubchak, Dr. A. D. Price and Dr. C. Sèguin is planned to be submitted.

Successful ideas are the result of slow growth. Ideas do not reach perfection in a day, no matter how much study is put upon them.

– Alexander Graham Bell

Dedication

Dedicated to my grandfather, Dr. Sci., Professor, and Mechanical Engineer, who instilled in my family a love for work and science.

Acknowledgements

Financial support for my studies was generously provided by Mitacs Canada, the Government of Ontario: Ministry of Research and Innovation, NSERC Canada, the Western Bone and Joint Institute, and Western University. Specifically, I would like to acknowledge the Mitacs Globalink program that gave me the opportunity to come to Canada and study at Western University. Special thanks to Oleksandr Romanko and Olena Skalianska for the enormous work they put towards making Mitacs internships possible for Ukrainian students.

Thank you to Dr. Maksym Pogorielov, Volodymyr Deineka, and everyone in the Biomaterials Research Centre at Sumy State University for involving me in their exiting research work during my undergraduate studies, and for their insightful guidance throughout my first steps in science.

Thank you to my supervisor, Dr. Aaron Price for his continual support, kindness and generosity, and for awarding me the freedom to pursue my research ideas. Thank you to the members of my Examination and Advisory Committees. Particulaty, thank you to Dr. Tom Appleton for his valuable insight and encouragement; to Dr. Cheryle Séguin for her guidance and thoughtful feedback, and for giving me the opportunity to connect with the world of medical and biological research.

Thank you to all my present and past colleagues in the Organic Mechatronics and Smart Materials Laboratory, and to all the members of the Séguin lab. Special thanks to Courtney Brooks for the countless hours of advice and assistance with cell culture work. Thank you to Matt Lawrence for his invaluable support throughout the years of Graduate School, and for sharing his experience that helped to navigate this project.

Special thank you to Ben Holness (and Murphy!), for being such an amazing friend and lab mate throughout the years, for his kindness and being here for me in the worst and best of times.

Thank you to my friends for their support during my journey in Canada. I owe special gratitude to my family: to my parents and grandparents for ensuring I have the best education and everything I need to pursue my goals and dreams; and to my siblings for their guidance and support.

I am eternally grateful for your kindness, friendship and support, thank you all.

Equity, Diversity & Inclusion (EDI)

Research and scientific knowledge are meant to be shared with everyone. The responsibility of students, teachers, researchers, trainees and others is to work on removing barriers and ensuring that knowledge and education are accessible for equity-deserving groups, which include but are not limited to women, Indigenous peoples (First Nations, Inuit, and Métis), members of racialized groups, persons with disabilities, and members of the LGBTQ2S+ community. My research does not focus on any population, demographic or health data. However, as a graduate student and a representative of a minority group myself (a female international student in Engineering), I have made my EDI commitments to be learning and accountability. Learning about other people's perspectives and experiences different from mine and stepping up to advocate for underrepresented groups in academia. Ultimately, the research we produce at Western needs to serve the diverse population of the Earth. It is our responsibility to create spaces for the knowledge and technological advancements to be accessible to everyone in the present, to build a healthier and safer world for our future generations.

Contents

List of Tables

List of Figures

List of Acronyms and Symbols

Acronyms

3D	three-dimensional
ANOVA	analysis of variance
APS	ammonuim persulfate
ASC	acetylsalicylic acid
BEMA-PEGMA	polyethylene glycolmethyl ether methacrylate
BMSCs	bone mesenchymal stem cells
BSA	bovine serum albumin
CE	counter electrode
CH	conducting hydrogels
CP	conducting polymer
CSA	chondroitin-4- sulphate
CV	cyclic voltammetry
DBSA	dodecylbenzene sulfonic acid
DLP	Direct Light Processing
DMEM	Dulbecco's Modified Eagle Medium
DoC	depth of cure
DPBS	Dulbecco's phosphate-buffered saline
DW	distilled water
ECM	extracellular matrix

ECP	electroactive conjugated polymers
FBS	fetal bovine serum
FESEM	field emission scanning electron microscopy
FI	fluorescein
FTIR	Fourier transform infrared spectroscopy
HA	hyaluronic acid
HepMA	heparin methacrylate
ICP	interfacial chemical polymerization
ISO	International Organization for Standardization
LAP	lithium-phenyl-2,4,6-trimethylbenzoylphosphinate
NIR	near-infrared radiation
NP	nanoparticles
NSA	naphthalene sulfonic acid
OA	osteoarthritis
OMASML	Organic Mechatronics and Smart Materials Laboratory
PANI	polyaniline
PBS	phosphate buffer saline
PCL	polycaprolactone
PDMS	polydimethylsiloxane
PEDOT	poly(3,4-ethylenedioxythiophene)
PEG	polyethylene glycol
PEGDA	poly(ethylene) glycol diacrylate
PEO	poly(ethylene oxide)
PFA	polyformaldehyde
PGA	poly(glycolic acid)
PI	photoinitiator
PLA	poly(lactic) acid

PPy	polypyrrole
PTMO	poly(tetramethylene oxide)
PTX	paclitaxel
PVA	polyvinyl alcohol
PVDF	poly(vinylidene) fluoride
RE	reference electrode
SDS	sodium dodecyl sulfate
SLA	stereolithography
SR	swelling ratio
TE	tissue engineering
TPO	diphenyl(2,4,6-trimethylbenzoyl)-phosphine oxide
UDMA	urethane dimethylacrylate
UV	ultra-violet
WE	working electrode

Greek symbols

χ	Flory-Huggin's interaction parameter
ρ	density
σ	conductivity
ξ	mesh size

Latin symbols

$\bar{v}$	specific volume
C_n	rigidity factor of a polymer
I	current
l	carbon-carbon bond length
m	mass
M_C	average molecular weight between crosslinks
M_N	average molecular weight

M_r	molecular weight of repeating units
Q_m	mass swollen ratio
r_0	end-to-end distance of the polymer in its free state
t	thickness
V	voltage
V_1	molar volume
$v_{2,r}$	polymer fraction, relaxed
$v_{2,s}$	polymer fraction, swollen

Chapter 1

Introduction

Articular cartilage lesions can occur due to traumatic injury to the joint or through the course of multifactorial joint diseases such as osteoarthritis (OA) (Hunziker, 2002). Unfortunately, the deterioration of articular cartilage in OA is not reversible, and chondral defects may penetrate to the bone and require joint replacement surgery (Wei and Dai, 2021). An additional precipitant to this problem is caused by the limited ability of cartilage tissue for self-repair and usually failed regeneration at the early stages of the disease (Wei and Dai, 2021).

Tissue engineering approaches combine biomaterials, cells and growth factors to generate an environment that can act as a replacement for injured cartilage and stimulate and support intrinsic regenerative processes. Biomaterials play an essential role as they are responsible for the mechanical stability of the tissue engineering construct and create a supportive environment for cells. For cartilage tissue engineering, hydrogels have been recognized as the one of the most promising biomaterials as they possess cartilage tissue-like features (Wei and Dai, 2021). Synthetic polymer hydrogels prepared with poly(ethylene) glycol diacrylate (PEGDA) have been studied and utilized for cartilage regeneration due to the ease in preparation and processing (Wei and Dai, 2021; Choi et al., 2019; Nguyen et al., 2013; Musumeci et al., 2011). PEGDA hydrogels have

the potential to be 3D printed into porous tissue engineering scaffolds using additive manufacturing technologies for photocurable polymers. However, they lack bioactivity and are intrinsically inert to cell adhesion and protein adsorption (Wei and Dai, 2021). The composites of PEGDA hydrogels with another synthetic or natural polymer have been proposed as a solution to this problem. Combining different materials into a composite allows superior physical properties and bioactivity (Wei and Dai, 2021).

The electroactive polymer polypyrrole (PPy) possesses a unique organic polymer property in the form of electrical conductivity. PPy has been extensively studied for use in tissue engineering as it can promote cell growth through electrical stimulation (Schmidt et al., 1997; Zhou et al., 2019). Additionally, PPy exhibits reversible electrochemistry, meaning it can be switched between the conductive and neutral states through the application of oxidative or reductive electrical potential accompanied by the ionic flow in and out of the polymer backbone (Schmidt et al., 1997). This property makes PPy an attractive material for controlled drug delivery applications, as it is capable of incorporating and releasing complex anionic compounds *on demand*.

Composite PEGDA-PPy materials have been previously introduced in the literature, however, they have been rarely studied for applications in drug delivery and regeneration of cartilage tissue. This thesis is a first-to-date systematic study providing the characterization of composite PEGDA-PPy hydrogels synthesized using interfacial chemical oxidative polymerization methods, as well as describing their drug delivery ability and potential for cartilage tissue engineering applications.

1.1 Objectives

This thesis aims to develop a conducting polymer-hydrogel biomaterial that can be utilized for drug delivery and support the regeneration of articular cartilage. The following objectives are required to achieve this goal:

- *Develop the manufacturing process for a biocompatible PEGDA-PPy biomaterial*

  It is desirable to control the properties of both components of the composite, and therefore a manufacturing process was developed to achieve this. In chapter 3 a modification to the interfacial chemical polymerization method is proposed to achieve higher conductivity, better electrochemical performance and surface modifications of the composite. Characterization of material was performed to investigate the impact of the conducting polymer phase on the structure and physical properties of the composite.

- *Develop a resin formulation to allow for 3D printing*

  The second objective was to tune the PEGDA hydrogel formulation with an addition of a biocompatible UV-absorber to be used in a custom designed stereolithography printer in the Organic Mechatronics and Smart Materials Laboratory (OMASML). Printing parameters were optimized to allow the printing of porous structures to target the production of tissue engineering scaffolds.

- *Develop an in-situ process for drug incorporation*

  The third objective was to develop the process that allows for drug incorporation during chemical oxidative polymerization. Drug release experiments are performed to prove the successful incorporation of the model drug compound and investigate possible triggers for controlled release.

- *Demonstrate the application of the composite biomaterial*

  The last objective was to demonstrate the application of the developed PEGDA-PPy biomaterial for controlled drug release and cell attachment. Time-dependant release of the model drug compound from the PEGDA-PPy were investigated. Biocompatibility and bioactivity of the developed composite were also reported.

1.2 Major contributions

This thesis communicates the following major contributions to the scientific community:

- *Novel interfacial chemical polymerization methods*

  This thesis represents first study that describes the modification of the interfacial chemical polymerization method for the creation of biocompatible PEGDA-PPy materials with improved physical properties and electrochemical performance.

- *A novel PEGDA resin formulation that allows for the creation of porous structures using 3D printing*

  The PEGDA resin described in this thesis enables the creation of lattice-like structures by means of an interfacial chemical polymerization method to obtain electroactive PEGDA-PPy hydrogels.

- *Characterization of the Fluorescein incorporation during chemical oxidative polymerization and its release from PEGDA-PPy materials*

  Here the first investigation into the doping of PPy during chemical oxidation is presented. The deprotonation of PPy in an alkaline environment demonstrated high release rates of the model drug compound and confirmed its incorporation. This research also provides insight into the pH-sensitivity of PEGDA hydrogels and Fluorescein and their contribution to drug delivery rates.

- *Biocompatibility and cell attachment studies of PEGDA-PPy hydrogels*

  Biocompatibility of the developed conducting hydrogels was confirmed via tests with the chondrogenic cell line ATDC5. Improved cell attachment and protein adsorption to the PEGDA-PPy materials prepared with the novel interfacial polymerization method were demonstrated.

1.3 Organization of the thesis

The following chapter, Chapter 2, *Background* summarizes the most influential knowledge in cartilage tissue structure, cartilage lesion pathology, and biomaterials used for cartilage repair. In accordance with the aforementioned objectives, the remainder of the thesis is organized as follows: Chapter 3, *PEGDA-PPy hydrogel fabrication* explores the fabrication and properties of PEGDA hydrogels and novel PEGDA-PPy composites, including the additive manufacturing of a PEGDA-PPy tissue engineering scaffold model. Next, Chapter 4, *Drug delivery from PEGDA-PPy hydrogels* explores the drug delivery capability of PEGDA-PPy biomaterials, specifically outlining the doping process during interfacial chemical polymerization and pH-sensitive drug release. Chapter 5, *PEGDA-PPy biocompatibility* describes biological studies used to validate the absence of toxicity from PEGDA and PEGDA-PPy hydrogels, and observe cell response to these materials. Finally, Chapter 6, *Concluding remarks* summarizes the conclusions of this work, reiterates the main scientific contributions, and provides recommendations for future research.

1.4 List of references

Choi, J. R., Yong, K. W., Choi, J. Y. and Cowie, A. C. (2019), 'Recent advances in photo-crosslinkable hydrogels for biomedical applications', *BioTechniques* **66**(1), 40–53.

Hunziker, E. B. (2002), 'Articular cartilage repair: Basic science and clinical progress. a review of the current status and prospects', *Osteoarthritis and Cartilage* **10**(6), 432–463.

Musumeci, G., Loreto, C., Carnazza, M. L., Strehin, I. and Elisseeff, J. (2011), 'Oa cartilage derived chondrocytes encapsulated in poly(ethylene glycol) diacrylate (PEGDA)

for the evaluation of cartilage restoration and apoptosis in an in vitro model', *Histology and Histopathology* **26**(10), 1265–1278.

Nguyen, A. K., Gittard, S. D., Koroleva, A., Schlie, S., Gaidukeviciute, A., Chichkov, B. N. and Narayan, R. J. (2013), 'Two-photon polymerization of polyethylene glycol diacrylate scaffolds with riboflavin and triethanolamine used as a water-soluble photoinitiator', *Regenerative Medicine* **8**(6), 725–738.

Schmidt, C. E., Shastri, V. R., Vacanti, J. P. and Langer, R. (1997), 'Stimulation of neurite outgrowth using an electrically conducting polymer', *Proceedings of the National Academy of Sciences of the United States of America* **94**(17), 8948–8953.

Wei, W. and Dai, H. (2021), 'Articular cartilage and osteochondral tissue engineering techniques: Recent advances and challenges', *Bioactive materials* **6**(12), 4830–4855.

Zhou, Z., Yu, P., Zhou, L., Tu, L., Fan, L., Zhang, F., Dai, C., Liu, Y., Ning, C., Du, J. and Tan, G. (2019), 'Polypyrrole nanocones and dynamic piezoelectric stimulation-induced stem cell osteogenic differentiation', *ACS Biomaterials Science and Engineering* **5**(9), 4386–4392.

Chapter 2

Background

The following chapter summarizes pertinent information about the structure and biomechanical characteristics of articular cartilage tissue gathered from the works of Alford and Cole (2005); Fox et al. (2009); Martinez-Moreno et al. (2019) and *Articular Cartilage* chapter of the book by Waters et al. (2018). The etiology and pathology of cartilage lesions, and challenges associated with cartilage tissue regeneration are discussed using the information from works by Alford and Cole (2005) and Hunziker (2002). Introduction to tissue engineering as a promising option for cartilage defect treatment is given. Electroactive conducting polymers (ECPs) are presented as biomaterials used in tissue engineering and regenerative medicine. Different methods used to fabricate composite ECP-containing materials are presented. Lastly, synthetic poly(ethylene) glycol-based hydrogels are discussed as materials used for cartilage tissue regeneration and drug delivery.

2.1 Cartilage tissue regeneration

2.1.1 Articular cartilage

Articular cartilage is a highly specialized connective tissue in a human body. It performs two major biomechanical functions in the joints. Firstly, articular cartilage creates a smooth layer on bone surfaces thus minimizing friction during motion. Secondly, it distributes compressive and tensile loads to the underlying subchondral bone. Complex composition and organization of articular cartilage contributes to its unique material properties that allow the tissue to withstand high constant compressive load.

Articular cartilage is a hyaline cartilage composing of extracellular matrix (ECM, occupies > 95 % of the tissue) and highly specialized cells called chondrocytes. The major components of extracellular matrix are water (> 80 % of the wet weight), collagen (type II) and proteoglycans. Negatively charged carboxyl and sulfate groups of proteoglycans ensure the high hydrophilicity of the ECM.

The content and organization of ECM components varies greatly through the cartilage layer thickness creating four major zones (fig. 2.1). The superficial zone has tightly packed and horizontally aligned collagen fibers responsible for the tensile properties of the tissue. The middle layer which occupies most of the tissue volume, contains cells and obliquely oriented collagen fibers, and serves as a first line of resistance for compression forces placed on the tissue. The deep zone has the lowest water content, but the largest proteoglycan concentration and is characterized by the perpendicular orientation of collagen fibers. This zone is responsible for providing resistance to the compression forces. The last calcified zone performs as a transition layer between cartilage and bone.

The excellent resilience of articular cartilage to compressive forces can be explained by the two-phase nature of the tissue. The porous structure of the solid ECM phase leads to the distribution of applied load due to the reduction in number of contact points.

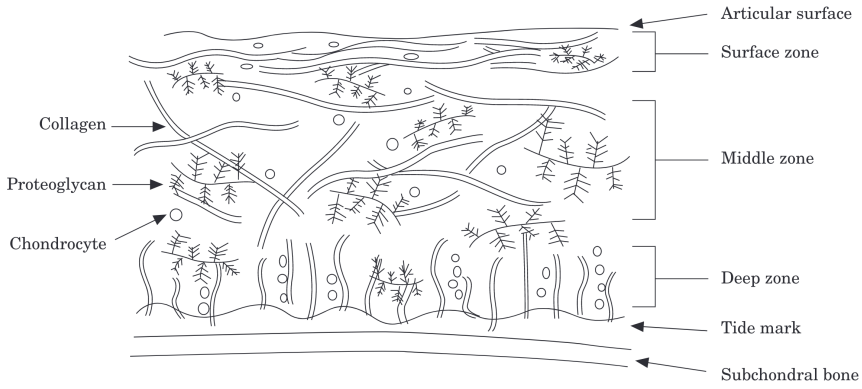

Figure 2.1: The structure of articular cartilage highlighting variations in orientation of the ECM components throughout the thickness of cartilage. © Setton et al. (1999), included with permission.

The flow of liquid phase (water) through the solid phase when compressive loads are applied contributes to the viscoelastic behaviour of the tissue. Low permeability of cartilage prevents water from being squeezed out of the matrix thus creating high fluid pressure which reduces the compressive load placed on the solid phase. While water moves through the charged regions of proteoglycans, it generates piezoelectric charges that further modulate liquid flow.

Articular cartilage lacks blood and lymphatic vessels, as well as innervation. Diffusion of nutrients from blood plasma happens mainly through the synovial fluid. The avascular nature of articular cartilage is greatly responsible for its limited ability to self-repair. Therefore, cartilage tissue lesions remain hard to treat.

2.1.2 Cartilage lesions

Articular cartilage lesions can occur either because of the injury or due to the degeneration of tissue caused by number of inflammatory joint diseases such as osteoarthritis (OA).

According to the Canadian Arthritis Society, OA is a multifactor pathology affecting nearly 6 million Canadians (Badley et al., 2019). This disease affects mostly large

weight-bearing joints in the human body such as knees, hips, lumbar and sacral spine, leading to significant limitations in mobility due to the subchondral bone sclerosis and high pain levels. The main pathological feature of OA is an inflammatory breakdown of the tissue due to action of proteolytic enzymes, followed by the loss of chondrocytes. Metabolic activity of the remaining cells is altered so that the catabolic processes prevail over the anabolic. As mentioned above, cartilage lesions have limited capacity for regeneration. Without specific treatment to suppress inflammatory processes and catabolic cell acitivity in OA, disease progresses and leads to the growth of the defect and bone tissue involvement.

However, different kinds of lesions possess various self-repair properties. In partial-thickness defects, only articular cartilage in the joint is affected. These injuries are usually characterized by the disruptions in cell metabolic activity and ECM composition. Full-thickness and osteochondral defects are deep cartilage defects that penetrate down to the subchondral bone. Osteochondral defects can penetrate as far as to the bone marrow. Full-thickness and osteochondral defects have some potential for spontaneous repair, contributed by the availability of stem cell sources, such as bone marrow, synovial fluid, blood vessels, adipose tissue and bone itself. These types of defects usually involve local bleeding and the formation of hematoma, and, subsequently, – fibrous cartilage tissue. However, this repair tissue has inferior biomechanical properties and will slowly deteriorate over time.

Currently available treatment options for these defects include surgical interventions and non-operative conservative therapies used to reduce symptoms and pain. Various surgical treatments involve the removal of affected tissue, and often stimulation of a spontaneous tissue healing response through the exposure of bone marrow, bone tissue (Hunziker, 2002). The most promising non-operative treatment options include cell-targeted therapies where therapeutic agents are injected to stimulate the build-up of the new cartilage tissues. However, all of them often result in the formation of

fibrocartilage that lacks mechanical stability to withstand compression loads (Falah et al., 2010; Jain and Ravikumar, 2020). The knowledge of cartilage structure and lesion pathology establishes considerations for the design of novel regenerative therapies for the treatment of cartilage lesions.

2.1.3 Cartilage tissue regeneration

Tissue engineering (TE), which combines biomaterials, cells and growth factors with an aim of restoration of the tissue, is a promising approach to provide long-term and stable repair of the cartilage. The basic principle behind TE is a utilization of a biomaterial matrix (TE scaffold) that provides structural support and biological cues for the cells during their attachment, proliferation and differentiation (Zhang et al., 2017; Pogorielov et al., 2017). Growth factors are used to induce or supress certain metabolic processes in cells thus regulating their behaviour (Jain and Ravikumar, 2020).

The biomaterial matrix plays an important role in TE as it supports and promotes the growth of the new tissue. The scaffold should be biocompatible, meaning it does not promote any (or only minimal) immune reaction. The main material requirements are sufficient porosity – to enable cell migration, nutrient/waste exchange, deformability and stiffness matching those of the tissue scaffold is aiming to replace (Hunziker, 2002; Jain and Ravikumar, 2020).

Ideally, the scaffold should be able to stimulate certain biological response from the cells (Hunziker, 2002; Zhang et al., 2017). This is particularly important for cartilage regeneration, as biological cues provided by the scaffold should stimulate formation of the hyaline cartilage as opposed to the fibrocartilage most frequently found at the place of injury. Additionally, the delivery of growth factors or other biologically active molecules from TE scaffold can possibly help to abolish inflammatory processes in OA cartilage lesions. Therefore, in TE, different modification techniques are used for surface treatments or to bind the material with certain biologically active molecules (e.g.

cell-adhesion promoting peptides such as RGD peptide) (Bellis, 2011).

Natural polymers (gelatin, collagen, chitosan, etc.) are usually the first choice for the fabrication of TE scaffolds (Zhang et al., 2017), however, synthetic polymers (poly(lactic) acid (PLA), poly(glycolic) acid (PGA), polyethylene glycol (PEG)-based, etc.) demonstrate better processability using additive manufacturing techniques for the creation of porous complex scaffold architectures (Pogorielov et al., 2017). The following section 2.2 and section 2.3 describe structural features and properties of electroactive organic polymers and synthetic hydrogels as promising candidates for tissue engineering applications.

2.2 Electroactive conjugated polymers (ECPs)

2.2.1 Structure and properties of ECPs

The first conducting organic polymer, polyacetylene, was synthesized and characterized in 1970 (Shirakawa et al., 1977). The Nobel Prize in Chemistry was awarded to Alan J. Heeger, Alan G. MacDiarmid and Hideki Shirakawa in 2000 “for the discovery and development of conductive polymers,” acknowledging the significant impact this discovery has made on the scientific community (Wan, 2008). As opposed to the majority of organic polymers, which are excellent insulators, conducting polymers have optical and physical properties of inorganic semiconductors and metals (Ferrigno et al., 2020). Since the discovery of polyacetylene, a number of conducting polymers (CPs) such as polypyrrole (PPy), polyaniline (PANI), and polythiophene have been developed as illustrated in fig. 2.2 (Holness, 2017). Their most common applications are in sensors and actuators (Ning et al., 2018); however, many research efforts have sought to utilize CPs for drug delivery and tissue regeneration.

The conductivity of CPs is enabled through their chemical structure. For example, polyacetylene, which might be considered the simplest example of a conjugated polymer,

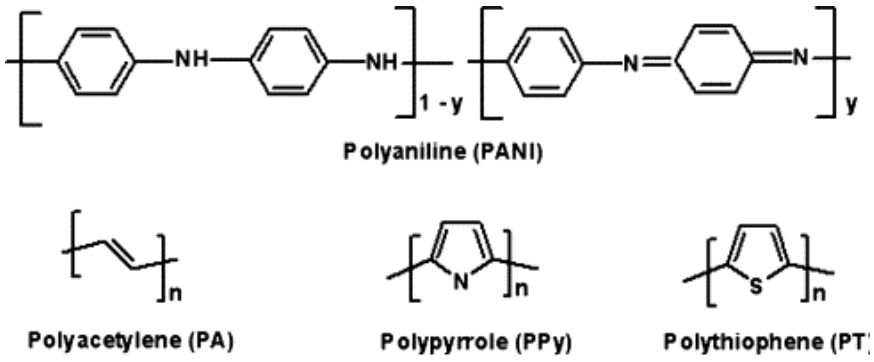

Figure 2.2: The chemical structure of various conducting polymers. Alternating single and double carbon bonds in the structure are responsible for the conductivity property. © Bhadra et al. (2009), included with permission.

has alternating single and double carbon bonds in its structure (fig. 2.2). Double bonds have overlapping π-electron waves (conjugation) of carbon atoms. These unpaired electrons can be delocalized through the polymer chain, thus allowing the electron flow and explaining the conductivity property of CPs (Wan, 2008; Le et al., 2017).

CPs exhibit a wide range of conductivity starting from an insulator ($10^{-10}\,\mathrm{S \cdot m^{-1}}$ to $10^{-8}\,\mathrm{S \cdot m^{-1}}$), to a semiconductor ($10^{-6}\,\mathrm{S \cdot m^{-1}}$ to $10\,\mathrm{S \cdot m^{-1}}$) and in some cases even exhibit metal-like conductivity ($10^{4}\,\mathrm{S \cdot m^{-1}}$). High conductivity is achieved through the doping process, and conductivity range depends on the degree of doping; conversely, in the undoped state, CPs behave as electrical insulators (Le et al., 2017). Doping entails the incorporation of ionic species into the polymer chain. As synthesized, CPs have an excessive positive charge and require a counter anion to maintain their electrochemical neutrality (fig. 2.3). Through the incorporation of a counter anion dopant, charge carriers are also introduced into the system. In case of PPy, charge carriers are called polarons and bipolarons. Electrons pass through the system when an electric potential is applied, and dopants move in or out of the polymer chain (Tandon et al., 2018).

Polypyrrole can be synthesized chemically and electrochemically from a pyrrole monomer. The polymerization mechanism involves the oxidation of pyrrole and coupling between radical cations (fig. 2.4), (Skotheim and Reynolds, 2006). The electrochemical

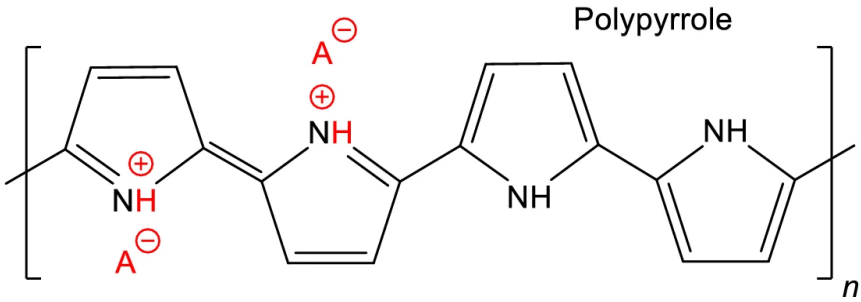

Figure 2.3: The chemical structure of polypyrrole. Anionic dopant is required to balance out the excessive positive charge of as-synthesized polymer. © Stejskal and Cz (2019), included with permission.

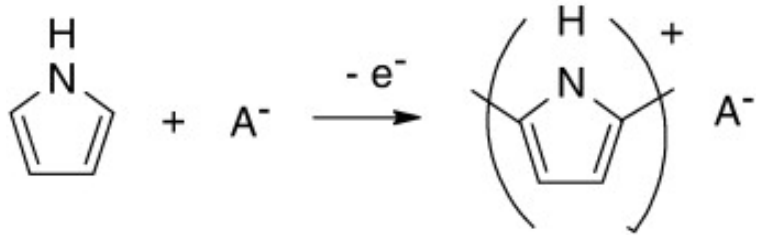

Figure 2.4: The oxidative polymerization of polypyrrole in the presence of anionic dopant. © Svirskis et al. (2010), included with permission.

method utilizes the application of an oxidative potential to initiate polymerization. In the chemical polymerization method, this function is performed by a strong oxidizing agent such as iron (III) chloride or ammonium persulfate (APS) (Ansari, 2006). The chemical oxidation method usually results in a precipitation of insoluble PPy powder, while electrochemical polymerization results in a deposition of PPy films on electrode surfaces, with both forms lacking mechanical stability (Miar et al., 2021).

2.2.2 Doping, drug incorporation and release

Doping of PPy with other molecules can be performed either chemically or electrochemically. In the case of chemical polymerization, dopants are usually limited to anions provided by oxidants. Every 3rd or 4th pyrrole unit in the polymer chain needs to be doped with a dopant anion for electrochemical stability (Ansari, 2006; Wallace et al., 2002). However, large anionic dopants can be successfully incorporated spontaneously

in competition with anions arising from the oxidant (Skotheim and Reynolds, 2006; Wallace et al., 2002). In work by Shen and Wan (1998), PPy was prepared via chemical oxidation with ammonium persulfate in the presence of different organic sulfonic acids. The resulting polymer powder was highly conductive and solvable in *m*-cresol as a result this approach.

The ability of CPs to uptake or release ionic molecules while being switched between oxidized and reduced states has been investigated for application in controlled drug delivery systems (Tandon et al., 2018). When the drug is incorporated into the CP structure as a dopant, the maximum loading that can be achieved is one drug molecule per 3 to 5 polymer monomer unints (Uppalapati et al., 2016).

The most studied way of drug doping is an electrochemical method. The medicinal compound can be loaded into the PPy via the one-step immobilization process during the electrochemical polymerization in the form of a primary dopant (Tandon et al., 2018). Successful doping of two clinically relevant drugs: dexamethasone and meropenem, with PPy during polymer deposition on the indium titan oxide coated glass electrodes was reported in work by Shah et al. (2018). In a study previously performed in the *Organic Mechatronics and Smart Materials Laboratory* (OMASML), Fluorescein (Fl) was successfully loaded into PPy films modified with microstructures during the electrochemical polymerization (Liubchak et al., 2020).

However, the disadvantages of a one-step method can include low drug loading capacity, inferior mechanical properties, and possible interferences to the polymerization process from the drug molecule (Tandon et al., 2018). An alternative to this is a three-step drug immobilization process which includes: 1) an electrochemical synthesis of PPy with the primary dopant of choice; 2) de-doping of PPy through the application of reduction potential; and 3) subsequent doping with the medicinal compound in an electrochemical cell (Tandon et al., 2018). In the study performed by Krukiewicz et al. (2015), both one-step and three-step drug incorporation methods were investigated

for their effectiveness in incorporating quercetin and ciprofloxacin. The post-synthesis approach has resulted in higher drug loading rates than the one-step doping process; however, the nature of the drug used for doping also played a significant role, as neutral quercetin was more effectively incorporated through the one-step approach.

Loading drug molecules during oxidative chemical polymerization usually happens via the one-step process, where a medicinal compound is added to the reaction mixture containing pyrrole monomer and oxidizer. Drugs are incorporated into the polymer structure along with the small anionic primary dopant provided by the oxidizer. PPy nanoparticles prepared via chemical oxidation demonstrated successful incorporation of anionic Fl and positively charged Rhodamine 6 G (R6G) in work by Samanta et al. (2015). The same research group also reports the incorporation and controlled release of clinically relevant protein insulin from PPy nanoparticles (Niloufar Hosseini-Nassab et al., 2016). Doping anti-tumour agent paclitaxel with PPy via oxidative chemical polymerization was successful in a study by Tiwari et al. (2018), where the drug was released using near-red irradiation (NIR) and showed an anticancer efficacy in an in vitro study with breast cancer cells.

To stimulate drug delivery from PPy, an oxidizing or reducing potential in an electrochemical cell can be applied. For example, electrical stimulation was used to release dexamethasone and penicillin/streptomycin from PPy films grown on titanium substrate (Sirivisoot et al., 2011). Almost 80 % of drugs were released using this method. Electrochemical stimulation was also effective for releasing neurotrophin-3, a protein that promotes the growth of various nerve cells (Thompson et al., 2006).

However, other factors, such as the pH of the environment, have been investigated as potential drug release triggers as well. The mechanism for the pH-sensitive dopant release from PPy has been extensively described in work by Samanta et al. (2015). Due to the excess of the hydrogen ions in as-synthesized PPy, in the alkaline media with low H^+ concentration, the polymer undergoes deprotonation reaction. Excess hydrogen

is released into the media, followed by the release of an anionic dopant to maintain polymer stability (Samanta et al., 2015). Based on the elemental analysis data, the hydrogen content of PPy (NO_3)-films is significantly reduced after they are immersed in the basic solution (Pei and Qian, 1991). The conductivity of PPy is also decreased when it's in the deprotonated state (Prokes et al., 2019).

In the strong acidic media, doped PPy undergoes a protonation reaction, followed by a slight increase in conductivity. In this case, the overall hydrogen ion content in PPy is increased, thus raising the overall positive charge of the polymer. This reaction is not suitable for the release of anionic compounds, moreover, if the media contains anions, they can be incorporated into PPy along with hydrogen ions to maintain the polymer chain stability (Pei and Qian, 1991). However, according to Samanta et al. (2015), acidic pH values caused the repulsion of positively charged R6G due to the excessive positive charge of the polymer.

2.2.3 PPy for tissue engineering

PPy has been extensively studied for its potential applications in tissue engineering and regenerative medicine due to its unique chemical and physical structure, surface topology, and ease of modification (Ateh et al., 2006; Ramanaviciene et al., 2007).

Numerous cell viability studies varying across the range of different body systems have previously demonstrated that PPy is a biocompatible polymer. For example, the extraction solutions from chemically synthesized PPy were used on nerve cells and have shown no impact on cell viability in the study by Wang et al. (2004). Cardiac progenitor cells isolated from adult mice were cultivated on electrochemically prepared PPy films doped with various dopants, and have demonstrated high cell counts (Gelmi et al., 2014). In the in vivo study performed by Ramanaviciene et al. (2007), PPy particles were injected in mice intraperitoneally and have shown no toxicity. These experimental results highlight the potential implementation of PPy across the body.

Incorporation of biologically active molecules such as growth factors, laminin peptides etc., into the structure of PPy can improve the interactions between CPs and cells (Green et al., 2010, 2012). In the study done by Li and Yu (2017), PPy films prepared electrochemically in the presence of RGD peptide (fragment from the laminin protein necessary for cell attachment) have demonstrated an improved adhesion and higher proliferation rates of the human lung cancer cells A549 compared to the undoped PPy films and the glass polymer deposition substrate. Another study on PPy films doped with RGD peptides has demonstrated a significantly higher attachment rate of differentiated osteoblasts Giglio et al. (2000). PPy prepared with hyaluronic acid (HA) has demonstrated excellent biocompatibility, cell attachment and growth rates in the in vitro study with rat-derived pheochromocytoma cells (PC-12) (Kim et al., 2018). Moreover, Kim et al. (2018) illustrate an increase in vascularization in tissues surrounding the PPy-HA implant in the in vivo study due to the HA doped with PPy being an important angiogenesis factor. PPy films prepared electrochemically and doped with chondroitin-4-sulphate (CSA) have supported the human fibroblast cell attachment in work by Moreno et al. (2008).

In cardiac and neural tissue engineering, where electrical stimulation of newly formed tissues is desired, having an intrinsically conducting substrate for cell growth is advantageous (Ferrigno et al., 2020). For example, electronic conduction through PPy films used as a substrate for PC-12 cells has enhanced the growth and spreading of cell neurites (Schmidt et al., 1997). Musculoskeletal tissues such as bone can also benefit from electrical stimulation. Bone is an intrinsically piezoelectric material as it generates potential when the load is applied (Ferrigno et al., 2020). In the study done by Zhou et al. (2019) PPy nanocones combined with poly(vinylidene) fluoride (PVDF) polymer were used to culture bone mesenchymal stem cells (BMSCs). PVDF was subjected to mechanical load and has generated electronic potential that has been transmitted to cells through PPy nanocones, and supported the attachment and growth of BMSCs.

2.2.4 Conducting composites

One of the major challenges associated with application of PPy in drug delivery and tissue engineering, is poor mechanical properties of the polymer. PPy is a brittle material and demonstrates brittle fracture behaviour, breaking at very little elongation during tensile testing (Murray et al., 1997). An additional drawback is the inability of PPy to be processed into complex three-dimensional shapes (Runge et al., 2010).

Mechanical stability of the polymer can be improved through different processing and manufacturing approaches. These include blending CPs with other polymers and composites (Green et al., 2012). Numerous PPy blends with other materials have been reported so far. For example, the aforementioned PPy doped with paclitaxel was deposited through chemical oxidative polymerization on electrospun polycaprolactone (PCL) fibers (Tiwari et al., 2018). A similar approach was used to functionalize PCL-fumarate fibers with PPy used for the electrical stimulation of PC-12 cells in a study by Moroder et al. (2011).

Significant attention has been drawn to the conducting hydrogels (CHs). These are hybrid materials containing conducting polymers and hydrogels. Hydrogels, discussed in detail in the following section 2.3.1, are three-dimensional polymer networks with a high-water content and favorable mechanical properties. The following approaches can be used to produce conducting hydrogels: 1) in situ polymerization of a CP during the formation of a hydrogel; 2) post-polymerization deposition of CP; and 3) a combination of the previous two (Xu et al., 2020).

An example of a CH prepared using the one-step method is a material with self-healing properties made through simultaneous mixing of pyrrole monomer with chitosan powder dissolved in acetic acid and an aqueous solution of oxidizer (Xu et al., 2018). The main drawback of this one-step process is that all components require different solvents. Pyrrole monomer is insoluble in water, while aqueous solution is required for the preparation of hydrophilic hydrogel (Xu et al., 2020).

A similar approach with limited applications due to solubility issues involves incorporation of freshly synthesized CP into a hydrogel formulation prior to its cross-linking. In the study by Guarino et al. (2013) aniline monomer with oxidizer and dopant were dissolved in water (aniline is water soluble) and mixed with PEGDA aqueous solution as the polymerization proceeded. This was followed by the exposure of the reaction mixture to UV-light to initiate the cross-linking of PEGDA and to form CHs used for the in vitro study with PC-12 cells and human mesenchymal stem cells.

Poor solubility of pyrrole leads to challenges in dispersion of the pyrrole/organic solvent mixture or PPy particles in the hydrogel matrix. Also, incorporation of the CP in the hydrogel precursor solution can interfere with polymerization process for hydrogels. For example, an addition of black-coloured PPy nanoparticles in precursor solution prior to hydrogel polymerization leads to an insufficient light absorption and impacted solidification (Lawrence, 2021).

In contrast, the post-polymerization approach takes advantage of the poor monomer solubility in water in combination with hydrogel hydrophilicity and includes the following steps: firstly, a hydrogel matrix is prepared; secondly, it is infiltrated with aqueous solution of the oxidizer (or with pyrrole monomer dissolved in the appropriate organic solvent), and subsequently, immersed in the monomer solution (or in the oxidant solution) to initiate the polymerization process and polymer deposition (Xu et al., 2020). As pyrrole is insoluble in water, but oxidizers, such as ammonium persulfate, are mostly insoluble in organic solvents, the polymerization reaction occurs at the water/organic solvent interface in a process known as *interfacial chemical polymerization* (ICP) (Skotheim and Reynolds, 2006). Although this technique is highly dependent on the diffusion rates of polymerization components inside the hydrogel matrix (Xu et al., 2020), it provides some level of control over the process. The deposition of the polymer on the interface inside the hydrogel infiltrated with solutions is favoured. The ICP approach was successfully employed in the study by Fantino et al. (2018) for the deposition of PPy inside 3D printed

honeycomb PEGDA hydrogels.

CPs can also be deposited in the hydrogel matrix via electrochemical polymerization. In this case, however, because hydrogel is used as a working electrode in electrochemical cell, its high conductivity has to be ensured. In the study by Green et al. (2012), polyvinyl alcohol-heparin methacrylate (PVA-HepMA) hydrogel was polymerized on a platinum disc electrode precoated with a poly(3,4-ethylenedioxythiophene) (PEDOT) film. This was followed by the continued electrodeposition of PEDOT within hydrogel matrix as polymer grew from the electrode surface coated with conducting film through the PVA-HepMA matrix. This composite material was used for the in vitro study with neural cell culture as a promising material for neural prosthetics. While the electrochemical polymerization process is suitable for the fabrication of biosensors and actuators, it remains challenging to perform the deposition of PPy within complex hydrogel architectures, such as those found in TE scaffolds.

Electroactivity of materials enabled through the addition of PPy has attracted great interest for applications of CHs in biosensors or in neural cell culture where the conductivity property is required. However, these materials can also serve as drug carrier components in drug delivery systems due to their capacity for oxidation/reduction upon application of an electrical potential. CHs can also be applied as bio-instructive materials for musculoskeletal tissue regeneration, as they support the transmission of endogenous electrical signals between cells (Gonzalez-Fernandez et al., 2019).

2.3 Hydrogels

2.3.1 PEGDA hydrogel properties

Hydrogels are one of the most common materials to be used in scaffold design for cartilage tissue regeneration. Hydrogels are three-dimensional polymer networks that have cartilage tissue-like material properties. Due to their high hydrophilicity, hydrogels

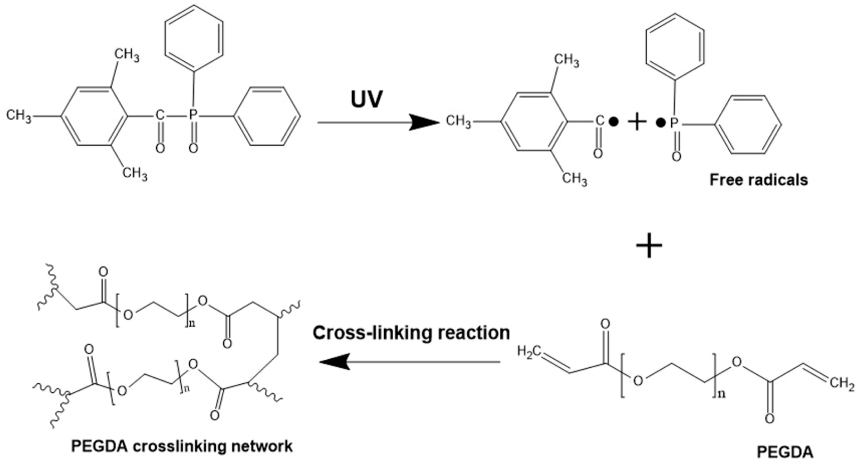

Figure 2.5: The scheme of light-sensitive polymerization of PEGDA hydrogel using the diphenyl(2,4,6-trimethylbenzoyl)-phosphine oxide (TPO) as a PI. © Yang et al. (2015), included with permission.

can absorb high amounts of water and provide resistance to the mechanical loads without any damage to their structure (Wei and Dai, 2021). Hydrogels can be divided into natural polymers (e.g. alginate, gelatin, collagen) and synthetic hydrogels ((PEG)-based materials, PVA, etc.).

Among synthetic hydrogels, PEGDA has gained significant attention in recent years for applications in drug delivery and tissue engineering due to the ease of preparation and modification. PEGDA is a photo-crosslinkable hydrogel, meaning light stimulus is needed to initiate the polymerization reaction. Crosslinking is induced through the addition of biocompatible photoinitiator (PI) in the presence of light source (fig. 2.5). Most commonly used biocompatible initiators are Irgacure 2959 and lithium-phenyl-2,4,6-trimethylbenzoylphosphinate (LAP), and both can be used with the UV light sources with wavelengths 320 nm to 390 nm (Choi et al., 2019).

PEGDA hydrogels have excellent mechanical properties which can be modulated based on the molecular weight and concentration of PEG precursors in the polymerization solution. Nguyen et al. (2013) have demonstrated how these parameters impact mechanical properties of PEGDA hydrogels. The confined compression modulusincreased with higher PEGDA concentrations and was in the range between 0.01 to

2.5 MPa, similar to the values for mature articular cartilage (0.19 to 2.1 MPa). Tensile modulus was found to be 0.02 to 3.5 MPa but was significantly lower than that of the mature cartilage tissue (4.8 to 25 MPa) and can be improved by the addition of another polymer or through fiber reinforcement.

Concentration and molecular weight of PEGDA precursors regulates the final crosslink density, which ultimately dictates not only the mechanical properties, but also network mesh size and swelling ratios. For example, in the study by Lin et al. (2011), PEGDA hydrogels with larger mesh size stimulated chondrocyte proliferation; however, they did not support the long-term accumulation of ECM components due to the large pore size and had the lowest compressive modulus.

The photopolymerizable nature of PEGDA enables the fabrication of hydrogels by means of additive manufacturing techniques, such as Stereolithography (SLA) and Direct Light Processing (DLP). These techniques use a focused laser or light projection onto a bath of photocurable resin and involve layer-by-layer growth of three-dimensional polymer structures. Both SLA and DLP offer high printing accuracy and extensive control over printing parameters and polymerization process (Mau et al., 2019). PEGDA hydrogel scaffolds loaded with acetylsalicylic acid (ASC) have been prepared using the SLA 3D printing method and used for the drug delivery study in the work by Vehse et al. (2014). This study, however, showed an increase in layer thickness within the prints due to high light penetration through the transparent PEGDA hydrogel, as well as a decrease in compressive modulus of printed PEGDA-ASC scaffolds due to the additional loading of drugs into the resin.

2.3.2 PEGDA hydrogel applications

PEGDA hydrogels have been previously used for encapsulation of OA derived chondrocytes and supported their growth and proliferation (Musumeci et al., 2011). They have also been used in in-vivo studies as materials to fill cartilage defects and stimulate

regeneration (Sharma et al., 2013). The main challenge in using these materials for cartilage regeneration remains in promoting the attachment of stem cells to the material and their subsequent proliferation. PEG materials are intrinsically resistant to cell adhesion and protein adsorption (Desai and Hubbell, 1991). The functionalization of hydrogels with specific molecules providing favourable conditions for stem cells has been proposed to overcome this obstacle, and incorporation of a co-polymer into the hydrogel material can improve binding with biologically active substances (Tamai et al., 2005).

PEGDA hydrogels can also be used for drug delivery. A significant work on PEG-based materials for drug release has been performed by Peppas et al. (1999). They have concluded that the mechanism of drug release from hydrogel is based on the diffusion of drug molecules from swollen polymer network, therefore is highly dependent on the mesh size and porosity of a material. Drugs are usually incorporated in PEGDA hydrogels prior to polymerization by dissolving them in the PEGDA precursor solution Vehse et al. (2014); McAvoy et al. (2018). There are several disadvantages associated with this process such as solubility of the drug of choice and its sensitivity to UV-light. Post-polymerization loading through swelling of ths hydrogel in the drug solution can be adversely impacted by the small mesh size. Therefore, creating a composite hydrogel with a co-polymer that can perform as a drug carrier can be advantageous. In this manner, the drug loading capacity of the composite will not depend on the microporosity of PEGDA, and drug release can be performed in a controlled rate.

2.4 Chapter summary

This chapter provided the necessary background information related to this research project. Structural, physiological and pathological features of cartilage tissues were discussed in relation to challenges in cartilage regeneration. Tissue engineering has

been introduced as a promising approach for treating cartilage tissue lesions. Finally, electroactive conducting polymers and hydrogels have been shown to exhibit many advantages that support their role in tissue regeneration.

2.5 List of references

Alford, J. W. and Cole, B. J. (2005), 'Cartilage restoration, part 1: Basic science, historical perspective, patient evaluation, and treatment options', *American Journal of Sports Medicine* **33**(2), 295–306.

Ansari, R. (2006), 'Polypyrrole conducting electroactive polymers: Synthesis and stability studies', *Journal of Chemistry* **3**(4), 186–201.

Ateh, D., Navsaria, H. and Vadgama, P. (2006), 'Polypyrrole-based conducting polymers and interactions with biological tissues', *Journal of The Royal Society Interface* **3**(11), 741–752.

Badley, E. M., Wilfong, J. M., Zahid, S. and Perruccio, A. V. (2019), The status of arthritis in canada: National report, Technical report, Arthritis Community Research and Evaluation Unit (ACREU), Prepared for the Arthritis Society.

Bellis, S. L. (2011), 'Advantages of RGD peptides for directing cell association with biomaterials', *Biomaterials* **32**(18), 4205–4210.

Bhadra, S., Khastgir, D., Singha, N. K. and Lee, J. H. (2009), 'Progress in preparation, processing and applications of polyaniline', *Progress in Polymer Science* **34**(8), 783–810.

Choi, J. R., Yong, K. W., Choi, J. Y. and Cowie, A. C. (2019), 'Recent advances in photo-crosslinkable hydrogels for biomedical applications', *BioTechniques* **66**(1), 40–53.

Desai, N. P. and Hubbell, J. A. (1991), 'Biological responses to polyethylene oxide modified polyethylene terephthalate surfaces', *Journal of biomedical materials research* **25**(7), 829–843.

Falah, M., Nierenberg, G., Soudry, M., Hayden, M. and Volpin, G. (2010), 'Treatment of articular cartilage lesions of the knee', *International Orthopaedics* **34**(5), 621.

Fantino, E., Roppolo, I., Zhang, D., Xiao, J., Chiappone, A., Castellino, M., Guo, Q., Pirri, C. F. and Yang, J. (2018), '3D printing/interfacial polymerization coupling for the fabrication of conductive hydrogel', *Macromolecular Materials and Engineering* **303**(4).

Ferrigno, B., Bordett, R., Duraisamy, N., Moskow, J., Arul, M. R., Rudraiah, S., Nukavarapu, S. P., Vella, A. T. and Kumbar, S. G. (2020), 'Bioactive polymeric materials and electrical stimulation strategies for musculoskeletal tissue repair and regeneration', *Bioactive Materials* **5**(3), 468–485.

Fox, A. J. S., Bedi, A. and Rodeo, S. A. (2009), 'The basic science of articular cartilage: Structure, composition, and function', *Sports Health* **1**(6), 461.

Gelmi, A., Ljunggren, M. K., Rafat, M. and Jager, E. W. (2014), 'Influence of conductive polymer doping on the viability of cardiac progenitor cells', *Journal of Materials Chemistry B* **2**(24), 3860–3867.

Giglio, E. D., Sabbatini, L., Colucci, S. and Zambonin, G. (2000), 'Synthesis, analytical characterization, and osteoblast adhesion properties on RGD-grafted polypyrrole coatings on titanium substrates', *Journal of Biomaterials Science, Polymer Edition* **11**(10), 1073–1083.

Gonzalez-Fernandez, T., Sikorski, P. and Leach, J. K. (2019), 'Bio-instructive materials for musculoskeletal regeneration', *Acta Biomaterialia* **96**, 20–34.

Green, R. A., Baek, S., Poole-Warren, L. A. and Martens, P. J. (2010), 'Conducting polymer-hydrogels for medical electrode applications', *Science and Technology of Advanced Materials* **11**(1), 014107.

Green, R. A., Hassarati, R. T., Goding, J. A., Baek, S., Lovell, N. H., Martens, P. J. and Poole-Warren, L. A. (2012), 'Conductive hydrogels: Mechanically robust hybrids for use as biomaterials', *Macromolecular Bioscience* **12**(4), 494–501.

Guarino, V., Alvarez-Perez, M. A., Borriello, A., Napolitano, T. and Ambrosio, L. (2013), 'Conductive PANi/PEGDA macroporous hydrogels for nerve regeneration', *Advanced Healthcare Materials* **2**(1), 218–227.

Holness, F. (2017), 'Additive manufacturing process of 3D polyaniline transducers via direct ink writing', *The University of Western Ontario Electronic Thesis and Dissertation Repository* **4849**.

Hunziker, E. B. (2002), 'Articular cartilage repair: Basic science and clinical progress. a review of the current status and prospects', *Osteoarthritis and Cartilage* **10**(6), 432–463.

Jain, K. and Ravikumar, P. (2020), 'Recent advances in treatments of cartilage regeneration for knee osteoarthritis', *Journal of Drug Delivery Science and Technology* **60**, 102014.

Kim, S., Jang, Y., Jang, M., Lim, A., Hardy, J. G., Park, H. S. and Lee, J. Y. (2018), 'Versatile biomimetic conductive polypyrrole films doped with hyaluronic acid of different molecular weights', *Acta Biomaterialia* **80**, 258–268.

Krukiewicz, K., Stokfisz, A. and Zak, J. K. (2015), 'Two approaches to the model drug immobilization into conjugated polymer matrix', *Materials Science and Engineering C* **54**, 176–181.

Lawrence, M. (2021), '3D printed polypyrrole scaffolds for pH dependent drug delivery with applications in bone regeneration', *The University of Western Ontario Electronic Thesis and Dissertation Repository* **7837**.

Le, T. H., Kim, Y. and Yoon, H. (2017), 'Electrical and electrochemical properties of conducting polymers', *Polymers* **9**(4), 150.

Li, Y. and Yu, C. (2017), 'RGD peptide doped polypyrrole film as a biomimetic electrode coating for impedimetric sensing of cell proliferation and cytotoxicity', *Journal of Applied Biomedicine* **15**(4), 256–264.

Lin, S., Sangaj, N., Razafiarison, T., Zhang, C. and Varghese, S. (2011), 'Influence of physical properties of biomaterials on cellular behavior', *Pharmaceutical Research* **28**(6), 1422–1430.

Liubchak, I., Lawrence, M. T., Holness, F. B. and Price, A. D. (2020), 'Soft template electropolymerization of polypyrrole for improved pH-induced drug delivery', *International Journal of Molecular Sciences* **21**(21), 8114.

Martinez-Moreno, D., Jiménez, G., Gálvez-Martín, P., Rus, G. and Marchal, J. A. (2019), 'Cartilage biomechanics: A key factor for osteoarthritis regenerative medicine', *Biochimica et Biophysica Acta - Molecular Basis of Disease* **1865**(6), 1067–1075.

Mau, R., Nazir, J., John, S. and Seitz, H. (2019), 'Preliminary study on 3D printing of PEGDA hydrogels for frontal sinus implants using digital light processing (DLP)', *Current Directions in Biomedical Engineering* **5**(1), 249–252.

McAvoy, K., Jones, D. and Thakur, R. R. S. (2018), 'Synthesis and characterisation of photocrosslinked poly(ethylene glycol) diacrylate implants for sustained ocular drug delivery', *Pharmaceutical Research* **35**(2), 1–17.

Miar, S., Ong, J. L., Bizios, R. and Guda, T. (2021), 'Electrically stimulated tunable drug delivery from polypyrrole-coated polyvinylidene fluoride', *Frontiers in Chemistry* **9**, 4.

Moreno, J. S., Panero, S., Artico, M. and Filippini, P. (2008), 'Synthesis and characterization of new electroactive polypyrrole-chondroitin sulphate a substrates', *Bioelectrochemistry* **72**(1), 3–9.

Moroder, P., Runge, M. B., Wang, H., Ruesink, T., Lu, L., Spinner, R. J., Windebank, A. J. and Yaszemski, M. J. (2011), 'Material properties and electrical stimulation regimens of polycaprolactone fumarate-polypyrrole scaffolds as potential conductive nerve conduits', *Acta Biomaterialia* **7**(3), 944–953.

Murray, P., Spinks, G. M., Wallace, G. G. and Burford, R. P. (1997), 'In-situ mechanical properties of tosylate doped (pts) polypyrrole', *Synthetic Metals* **84**, 847–848.

Musumeci, G., Loreto, C., Carnazza, M. L., Strehin, I. and Elisseeff, J. (2011), 'Oa cartilage derived chondrocytes encapsulated in poly(ethylene glycol) diacrylate (PEGDA) for the evaluation of cartilage restoration and apoptosis in an in vitro model', *Histology and Histopathology* **26**(10), 1265–1278.

Nguyen, A. K., Gittard, S. D., Koroleva, A., Schlie, S., Gaidukeviciute, A., Chichkov, B. N. and Narayan, R. J. (2013), 'Two-photon polymerization of polyethylene glycol diacrylate scaffolds with riboflavin and triethanolamine used as a water-soluble photoinitiator', *Regenerative Medicine* **8**(6), 725–738.

Niloufar Hosseini-Nassab, Devleena Samanta, Yassan Abdolazimi, P. Annes, J. and N. Zare, R. (2016), 'Electrically controlled release of insulin using polypyrrole nanoparticles', *Nanoscale* **9**(1), 143–149.

Ning, C., Zhou, Z., Tan, G., Zhu, Y. and Mao, C. (2018), 'Electroactive polymers for tissue regeneration: Developments and perspectives', *Progress in Polymer Science* **81**, 144–162.

Pei, Q. and Qian, R. (1991), 'Protonation and deprotonation of polypyrrole chain in aqueous solutions', *Synthetic Metals* **45**(1), 35–48.

Peppas, N. A., Keys, K. B., Torres-Lugo, M. and Lowman, A. M. (1999), 'Poly(ethylene glycol)-containing hydrogels in drug delivery', *Journal of Controlled Release* **62**, 81–87.

Pogorielov, M., Oleshko, O. and Hapchenko, A. (2017), 'Tissue engineering: challenges and selected application', *Advances in Tissue Engineering & Regenerative Medicine: Open Access* **3**(2), 330–334.

Prokes, J., Varga, M., Vrňata, M., Valtera, S., Stejskal, J. and Kopecký, D. (2019), 'Nanotubular polypyrrole: Reversibility of protonation/deprotonation cycles and long-term stability', *European Polymer Journal* **115**, 290–297.

Ramanaviciene, A., Kausaite, A., Tautkus, S. and Ramanavicius, A. (2007), 'Biocompatibility of polypyrrole particles: an in-vivo study in mice', *The Journal of pharmacy and pharmacology* **59**(2), 311–315.

Runge, M. B., Dadsetan, M., Baltrusaitis, J., Knight, A. M., Ruesink, T., Lazcano, E. A., Lu, L., Windebank, A. J. and Yaszemski, M. J. (2010), 'The development of electrically conductive polycaprolactone fumarate-polypyrrole composite materials for nerve regeneration', *Biomaterials* **31**(23), 5916–5926.

Samanta, D., Meiser, J. L. and Zare, R. N. (2015), 'Polypyrrole nanoparticles for tunable, pH-sensitive and sustained drug release', *Nanoscale* **7**(21), 9497–9504.

Schmidt, C. E., Shastri, V. R., Vacanti, J. P. and Langer, R. (1997), 'Stimulation of neurite outgrowth using an electrically conducting polymer', *Proceedings of the National Academy of Sciences of the United States of America* **94**(17), 8948–8953.

Setton, L. A., Elliot, D. M. and Mow, V. C. (1999), Altered mechanics of cartilage with osteoarthritis: human osteoarthritis and an experimental model of joint degeneration, Technical report.

Shah, S., Firlak, M., Berrow, S., Halcovitch, N., Baldock, S., Yousafzai, B., Hathout, R. and Hardy, J. (2018), 'Electrochemically enhanced drug delivery using polypyrrole films', *Materials* **11**(7), 1123.

Sharma, B., Fermanian, S., Gibson, M., Unterman, S., Herzka, D. A., Cascio, B., Coburn, J., Hui, A. Y., Marcus, N., Gold, G. E. and Elisseeff, J. H. (2013), 'Human cartilage repair with a photoreactive adhesive-hydrogel composite', *Science Translational Medicine* **5**(167), 167ra6–167ra6.

Shen, Y. and Wan, M. (1998), 'In situ doping polymerization of pyrrole with sulfonic acid as a dopant', *Synthetic Metals* **96**(2), 127–132.

Shirakawa, H., Louis, E. J., MacDiarmid, A. G., Chiang, C. K. and Heeger, A. J. (1977), 'Synthesis of electrically conducting organic polymers: halogen derivatives of polyacetylene, $(CH)_x$', *Journal of the Chemical Society, Chemical Communications* (16), 578–580.

Sirivisoot, S., Pareta, R. and Webster, T. J. (2011), 'Electrically controlled drug release from nanostructured polypyrrole coated on titanium', *Nanotechnology* **22**(8), 085101.

Skotheim, T. A. and Reynolds, J. R., eds (2006), *Conjugated polymers: theory, synthesis, properties, and characterization*, Handbook of Conducting Polymers, Fourth Edition, 3rd edn, CRC Press, Boca Raton, FL.

Stejskal, J. and Cz, S. C. (2019), 'Interaction of conducting polymers, polyaniline and polypyrrole, with organic dyes: polymer morphology control, dye adsorption and photocatalytic decomposition', *Chemical Papers 2019 74:1* **74**(1), 1–54.

Svirskis, D., Travas-Sejdic, J., Rodgers, A. and Garg, S. (2010), 'Electrochemically controlled drug delivery based on intrinsically conducting polymers', *Journal of Controlled Release* **146**(1), 6–15.

Tamai, N., Myoui, A., Hirao, M., Kaito, T., Ochi, T., Tanaka, J., Takaoka, K. and Yoshikawa, H. (2005), 'A new biotechnology for articular cartilage repair: Subchondral implantation of a composite of interconnected porous hydroxyapatite, synthetic polymer (PLA-PEG), and bone morphogenetic protein-2 (rhbmp-2)', *Osteoarthritis and Cartilage* **13**(5), 405–417.

Tandon, B., Magaz, A., Balint, R., Blaker, J. J. and Cartmell, S. H. (2018), 'Electroactive biomaterials: Vehicles for controlled delivery of therapeutic agents for drug delivery and tissue regeneration', *Advanced Drug Delivery Reviews* **129**, 148–168.

Thompson, B. C., Moulton, S. E., Ding, J., Richardson, R., Cameron, A., O'Leary, S., Wallace, G. G. and Clark, G. M. (2006), 'Optimising the incorporation and release of a neurotrophic factor using conducting polypyrrole', *Journal of Controlled Release* **116**(3), 285–294.

Tiwari, A. P., Hwang, T. I., Oh, J.-M., Maharjan, B., Chun, S., Kim, B. S., Joshi, M. K., Park, C. H. and Kim, C. S. (2018), 'pH/NIR-responsive polypyrrole-functionalized fibrous localized drug-delivery platform for synergistic cancer therapy', *ACS Applied Materials & Interfaces* **10**(24), 20256–20270.

Uppalapati, D., Boyd, B. J., Garg, S., Travas-Sejdic, J. and Svirskis, D. (2016), 'Conducting polymers with defined micro- or nanostructures for drug delivery', *Biomaterials* **111**, 149–162.

Vehse, M., Petersen, S., Sternberg, K., Schmitz, K. P. and Seitz, H. (2014), 'Drug delivery from poly(ethylene glycol) diacrylate scaffolds produced by dlc based microstereolithography', *Macromolecular Symposia* **346**(1), 43–47.

Wallace, G. G., Teasdale, P. R., Spinks, G. M. and Kane-Maguire, L. A. P. (2002), 'Conductive electroactive polymers : Intelligent materials systems, second edition', *Conductive Electroactive Polymers* .

Wan, M. (2008), 'Conducting polymers with micro or nanometer structure', *Conducting Polymers with Micro or Nanometer Structure* pp. 1–292.

Wang, X., Gu, X., Yuan, C., Chen, S., Zhang, P., Zhang, T., Yao, J., Chen, F. and Chen, G. (2004), 'Evaluation of biocompatibility of polypyrrole in vitro and in vivo', *Journal of Biomedical Materials Research Part A* **68A**(3), 411–422.

Waters, T. S., Heidari, N. and Bentley, G. (2018), 'Articular cartilage', *Basic Orthopaedic Sciences* pp. 147–158.

Wei, W. and Dai, H. (2021), 'Articular cartilage and osteochondral tissue engineering techniques: Recent advances and challenges', *Bioactive materials* **6**(12), 4830–4855.

Xu, J., Tsai, Y. L. and Hsu, S. H. (2020), 'Design strategies of conductive hydrogel for biomedical applications', *Molecules (Basel, Switzerland)* **25**(22), 5296.

Xu, T., Chu, M., Wu, Y., Liu, J., Chi, B., Xu, H., Wan, M. and Mao, C. (2018), 'Safer cables based on advanced materials with a self-healing technique that can be directly powered off and restored easily at any time', *New Journal of Chemistry* **42**(7), 4803–4806.

Yang, W., Yu, H., Liang, W., Wang, Y. and Liu, L. (2015), 'Rapid fabrication of hydrogel microstructures using UV-induced projection printing', *Micromachines 2015, Vol. 6, Pages 1903-1913* **6**(12), 1903–1913.

Zhang, Y. S., Yue, K., Aleman, J., Mollazadeh-Moghaddam, K., Bakht, S. M., Yang, J., Jia, W., Dell'Erba, V., Assawes, P., Shin, S. R., Dokmeci, M. R., Oklu, R. and

Khademhosseini, A. (2017), '3D bioprinting for tissue and organ fabrication', *Annals of biomedical engineering* **45**(1), 148.

Zhou, Z., Yu, P., Zhou, L., Tu, L., Fan, L., Zhang, F., Dai, C., Liu, Y., Ning, C., Du, J. and Tan, G. (2019), 'Polypyrrole nanocones and dynamic piezoelectric stimulation-induced stem cell osteogenic differentiation', *ACS Biomaterials Science and Engineering* **5**(9), 4386–4392.

Chapter 3

Fabrication and Characterization of Composite Poly(ethylene) Glycol Diacrylate - Polypyrrole Hydrogels

This chapter outlines the development of a composite PEGDA-PPy biomaterial. A multistep approach is used to incorporate conducting polymer into the photocurable PEGDA hydrogel matrix. This process includes a UV-light-initiated crosslinking of PEGDA, followed by the interfacial chemical polymerization of PPy. Chemical structure and physical properties of PEGDA matrix and composite PEGDA-PPy hydrogel are investigated. DLP 3D printing technology was used to create a porous PEGDA matrix, subsequently used for PPy deposition. Lastly, surface morphology of PEGDA hydrogels and PEGDA-PPy composites is compared using optical and SEM imaging.

3.1 Introduction

As described in section 2.2.4, chemical and electrochemical methods used for polymerization of pyrrole yield a polymer lacking mechanical stability. In order to exploit the

advantageous properties of PPy and create a biomaterial having the mechanical properties required for use in regeneration of musculoskeletal tissues, it can be blended into a composite with other polymers, such as hydrogels. This thesis explores the creation of a biocompatible composite PEGDA-PPy material. The choice of PEGDA hydrogel as a deposition matrix for PPy is motivated by the ease and feasibility of PEGDA preparation. PEGDA can be polymerized through the exposure of oligomer formulation to the UV-light. Free radicals are generated from photoinitiators added to the formulation and they start the polymerization reaction (Uttayarat et al., 2016). UV-light is considered to be a great external stimuli as it can be easily switched on and off and allows to control the reaction in a timely and spatial manner (Choi et al., 2019). One of the possible drawbacks behind using photocurable hydrogels is a possible cytotoxic effect of free radicals generated during polymerization reaction (Fedorovich et al., 2009).

In work previously performed in the OMASML, PPy nanoparticles (PPy NPs) synthesized via oxidative chemical polymerization using the method described by Samanta et al. (2015) were incorporated into a PEGDA hydrogel (Lawrence, 2021). This was achieved by adding a NP suspension to a PEGDA oligomer formulation. The resulting photocurable PEGDA-PPy NP resin formulation was exposed to UV-light to produce biocompatible CHs used for drug delivery and cell attachment studies. Additionally, this formulation was evaluated for the 3D printing of a bone graft model using a specialized DLP technique developed in the OMASML.

A specially-developed additive manufacturing system located in the OMASML is tailored to produce micro- and nanoscale features with CP resin formulations. The important components of the printer are the DLP light engine and a vat filled with polymer resin formulation fig. 3.1. The DLP generates light patterns which are displayed on the liquid surface for the prescribed cure time, and selectively polymerize and solidify polymer formulation layers (Cullen and Price, 2018). The vat then moves down leaving the fresh layer of resin exposed to the light pattern, and the process is repeated until

the desired geometry and architecture is produced. Cullen and Price (2018) were able to utilize this technology to produce microscale 3D CP structures. Multi-material resin formulation containing urethane dimethylacrylate (UDMA) as a base polymer, pyrrole, silver nitrate and PI H-Nu 470 was used, where PI generates free radicals which initiate polymerization reaction for UDMA and sensitize cationic initiator silver nitrate to start the polymerization of pyrrole (Cullen and Price, 2018). A similar approach was used in work by Cullen and Price (2019) and by Holness et al. (2021) to produce 3D CP transducers but the UDMA polymer was replaced with a blend of bisphenol A ethoxylate dimethacrylate and polyethylene glycolmethyl ether methacrylate (BEMA-PEGMA) copolymer. However, these formulations are not biocompatible due to the addition of silver nitrate.

As described by Lawrence (2021), PEGDA-PPy NPs resin formulation was found to be biocompatible and demonstrated good 3D printing capabilities. PEGDA resin omitting any PPy NPs (0 %) showed significant overcuring. At the same time, other resin formulations containing PPy NPs showed high print resolutions due to the ability of NPs to absorb excess light. However, higher concentrations of NPs led to undercuring due to the high rates of light absorption.

Given the limitations to PPy loading in 3D-printed structures, post-polymerization approaches for CP deposition, namely the interfacial chemical polymerization outlined in section 2.2.4, was chosen to prepare PEGDA-PPy samples in this work. A novel modification to the ICP method is presented in this thesis. The conductivity and electrochemical performance of PEGDA-PPy hydrogels prepared with a modified method were significantly improved. The chemical structure and physical properties of hydrogels such as swelling ratio were investigated prior and following polymerization. For 3D printing scaffolds, PEGDA resin formulation with an addition of UV-absorber was developed and its printing capabilities were characterized prior to PPy deposition.

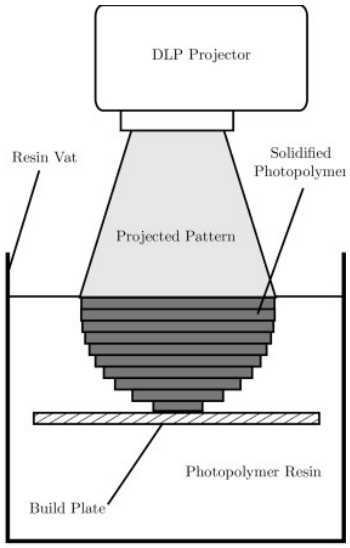

Figure 3.1: DLP free-surface 3D printing technology used for the fabrication of micro- and nanoscale features with photopolymerizable resin formulations. © Cullen and Price (2018), included with permission.

3.2 Materials and Methods

3.2.1 PEGDA hydrogel polymerization and characterization

To prepare the hydrogel matrix, a PEGDA formulation was developed as follows: firstly, biocompatible photoinitiator LAP (CAS #85073-19-4) was dissolved in distilled water (DW) in an amount of $0.5\,\mathrm{mg}\cdot\mathrm{mL}^{-1}$ (0.05 % (w/v)). Secondly, PEGDA oligomer formulation (average M_n 700, CAS #26570-48-9) was mixed with a LAP solution in various PEGDA ratios: 20, 30, 40, 50, 60, 70 and 80 % (w/v). Different PEGDA concentrations were used to investigate the differences in physical properties of hydrogels. The PEGDA formulation was then poured into a 1 cm×1.5 cm polydimethylsiloxane (PDMS) mold and exposed to the UV-light (λ = 405 nm) for 10 min. After exposure, solidified PEGDA samples were thoroughly washed with DW three times and left to dry overnight before proceeding with subsequent characterization or PPy deposition.

To investigate the physical properties of PEGDA hydrogels containing different

PEGDA concentrations, their swelling ratios (SR) in DW were evaluated. Additionally, SRs of PEGDA in phosphate buffer saline (PBS) (pH 7.45), buffer solutions with pH values of 8, 10, 12 and 13 were also calculated. Each sample's dry mass was measured, and subsequently placed in an individual vial filled with a selected solution (DW, PBS, etc.), and left overnight. The following day, samples were carefully removed from the solution and any excess liquid was wiped out from the surface prior to measuring the swollen mass. Swelling ratios were calculated according to:

$$\text{Swelling Ratio} = \frac{m_s - m_d}{m_d}, \tag{3.1}$$

where m_s is the mass of the swollen hydrogel and m_d is the mass of the dried hydrogel before swelling.

Based on the swelling properties of the hydrogel in DW, crosslink density was evaluated by calculating average molecular weight between the crosslinks ($\overline{M_c}$,) using the Peppas-Merrill model and formulas given below (Lee et al., 2000; Lin et al., 2011; Koetting et al., 2015):

$$\frac{1}{\overline{M_c}} = \frac{2}{\overline{M_n}} - \frac{\left(\bar{v}/V_1\right)\left[\ln\left(1 - v_{2,\,s}\right) + v_{2,\,s} + \chi_1 v_{2,\,s}^2\right]}{v_{2,r}\left[\left(\frac{v_{2,s}}{v_{2,r}}\right)^{1/3} - \frac{v_{2,s}}{2v_{2,r}}\right]}, \tag{3.2}$$

where $\overline{M_n}$ is the average weight of the PEGDA (700 Mn), $\bar{v}$ is the specific volume of PEGDA ($0.893\,\text{cm}^3 \cdot \text{g}^{-1}$), V_1 is the molar volume of water ($18\,\text{cm}^3 \cdot \text{g}^{-1}$), χ_1 is the Flory-Huggin's PEG-water interaction parameter (0.426), $v_{2,r}$ is the polymer fraction (0.2, 0.4 or 0.8) and $v_{2,s}$ is the polymer volume fraction in the swollen state, as defined by:

$$v_{2,s} = \frac{\frac{1}{\rho_2}}{\frac{Q_m}{\rho_1} + \frac{1}{\rho_2}}, \tag{3.3}$$

where ρ_1 and ρ_2 are the density of the solvent and PEGDA respectively and Q_m is the

mass swelling ratio.

Mesh sizes (ξ) of the PEGDA hydrogels were calculated according to the formula:

$$\xi = \left(\overline{r_0^2}\right)^{1/2} v_{2,\,s}^{-1/3}, \tag{3.4}$$

where r_0^2 was determined by:

$$\overline{r_0^2} = l^2 \left[2\frac{\overline{M_c}}{M_r}\right] C_n, \tag{3.5}$$

where l is a carbon-carbon bond length(0.154 nm), C_n is the rigidity factor of polymer (4 for PEG), and M_r is the molecular weight of repeating units ($44\,\mathrm{g \cdot mol^{-1}}$ for PEG).

3.2.2 PEGDA-PPy material fabrication and characterization

For the preparation of conducting PEGDA-PPy hydrogels, interfacial chemical polymerization method was used, introduced in section 2.2.4. Briefly, this method includes subsequent submerging of PEGDA matrix in solutions of oxidizer and pyrrole. A modification of this method was introduced in this thesis to produce two different kinds of samples, referenced below as PEGDA-PPy-a and PEGDA-PPy-b.

For PEGDA-PPy-a, dried PEGDA matrices containing 20, 40 and 80% (w/v) PEGDA were placed in a 0.14 mol aqueous solution of the oxidizer APS (CAS #7727-54-0) for 2 h to allow the diffusion of oxidizer into the hydrogel. Samples were then removed from the solution, excessive liquid was wiped out from their surface, and they were carefully placed in a different vial filled with freshly distilled pyrrole monomer (CAS #109-97-7) dissolved in cyclohexane (0.1 mol). The polymerization reaction occurs rapidly as indicated by the colour change of the hydrogel from transparent to black. Samples were left in a solution for an hour, then removed and any excess monomers and solvents were washed from the surface with 70 % ethanol. Samples were then dried overnight prior to any characterization or further studies.

For PEGDA-PPy-b, dried PEGDA hydrogels were first placed in the solution of

pyrrole, followed by the soak in APS solution. The molarity, solvents, reaction time, and post-polymerization wash remained the same as for the PEGDA-PPy-a. Reversing polymerization steps in this case was found to yield samples with different surface morphology.

The polymer product of ICP was also produced separately. In a beaker, 5 mL of the 0.14 mol aqueous solution of APS were combined with 5 mL of 0.1 mol of pyrrole in cyclohexane under constant magnetic stirring. The reaction happens immediately and results in the precipitation of insoluble PPy particles. Particles were paper-filtrated and washed with ethanol, then left to dry in the fume hood overnight. This method has also been used to prepare PPy particles doped with Fl for the drug delivery studies reported in section 4.2.

To confirm incorporation of a conducting component into the inert hydrogel matrix, the electrical conductivity of dried samples was measured with a four-point probe method using a Keithley 2611 source meter and a custom MATLAB script. Voltage measurements were taken over a span of 50 s from 3 different locations on 3 samples. The following equation was used to calculate conductivity:

$$\sigma = \frac{I \ln 2}{\pi \Delta V t}, \tag{3.6}$$

where σ is the apparent conductivity, I is the current applied between the first and fourth electrodes, ΔV is the recorded voltage drop between the second and third electrodes and t is thickness.

PEGDA hydrogels, PPy powder and PEGDA-PPy-a samples were analyzed with Fourier transform infrared (FTIR) spectroscopy using a Bruker Tensor II spectrometer. Swelling ratios of PEGDA-PPy samples were measured and calculated using the methodology described above for PEGDA hydrogels (section 3.2.1) to investigate the impact of a second polymer fraction on the physical properties of the composite.

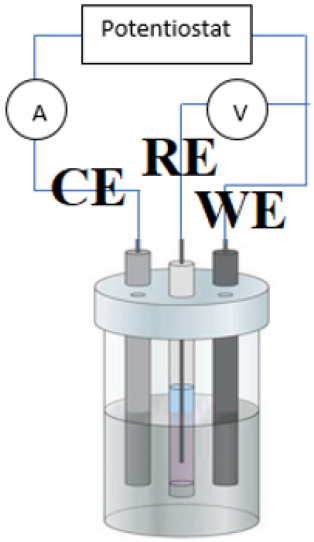

Figure 3.2: A three-electrode electrochemical cell used for cyclic voltammetry. Current is applied to the stainless steel counter electrode (CE), and the response is collected from the PEGDA-PPy working electrode (WE). © Taha et al. (2020), included with permission.

To evaluate the electrochemical performance of PEGDA-PPy hydrogels, cyclic voltammograms were recorded. Samples were connected to the source meter and used as working electrodes (WE) in a 3-electrode electrochemical cell also containing a stainless steel counter electrode (CE) and a silver-silver chloride reference electrode (RE) (fig. 3.2). The electrochemical cell was filled with a 0.1 mol aqueous sodium nitrate ($NaNO_3$) solution, and the potential was cycled between –0.5 V to 1.5 V for 5 cycles at a scan rate of $20\,mV \cdot s^{-1}$.

The surface morphology of the PEGDA, PEGDA-PPy-a and PEGDA-PPy-b samples was analyzed by means of a Keyence VHX-7000 digital microscope and Field Emission Scanning Electron Microscopy (FESEM).

All data was collected in triplicate (n=3) unless stated otherwise, to determine mean values and their associated standard deviations (±). One-way analysis of variance (ANOVA) and multiple comparison tests were performed using MATLAB.

3.2.3 3D printing

3D printing of PEGDA hydrogels was performed using the additive manufacturing technology outlined in section 3.1. 3D structures were produced using the custom-designed OMASML DLP printer, which has an emission wavelength of 385 nm, irradiation energy of $7.37\,\mathrm{J}\cdot\mathrm{cm}^{-3}$, and a theoretical minimum XY feature resolution of 5 µm. Prior to printing, depth of cure (DoC) tests were performed on several resin formulations to select the best formulation and establish the optimal layer cure time and layer thickness for 3D printing. All characterized PEGDA resin formulations contained 40 % (w/v) PEGDA, and 0.1 or 0.05 % (w/v) of LAP, and 0.5 , 0.75 , or 1 % (w/v) of UV-absorber Orange G dye (Sigma Aldrich Cat. #O3756). UV-absorbance of resin formulation components was collected using the Cary-60 spectrometer.

DoC experiments were performed as follows: a metal vat was filled with resin and covered with a transparent plastic microscope slide, so that there was a direct contact between the slide and the top layer of resin liquid. A metal vat was placed directly under the light engine of the printer and the light pattern illustrated in fig. 3.9 (a) was projected onto the slide for 5 s for the 0.1 % (w/v) LAP resin formulation, and for 10 s for the 0.05 % (w/v) LAP formulation. Six square features are projected on the first layer, and one feature is removed from the projection image with each subsequent exposure. In this way, every feature of the pattern is cured for a different amount of time creating varying layer thicknesses. The thickness of printed features was measured with Keyence VHX-7000 digital microscope, and correlated with UV-absorber concentrations creating a logarithmic trendline ($y = m_1 \ln x + C$), where average depth of cure was defined as the slope value m_1.

Following DoC tests and resin formulation selection, the following parameters were prescribed for 3D printing: 100 µm layer thickness and 40 s cure time. Four base layers of unpatterned film and one additional base layer of features, each cured for 120 s, were required due to printer setup to avoid variations in first layer thicknesses. To test

feature resolution that can be achieved with selected resin formulation, pattern outlined in fig. 3.10 (a) (adapted from Thingiverse #2011862) was printed. Other print models were designed using either the SolidWorks or nTopology software (fig. 3.11 (a–b)).

3.3 Results and Discussion

3.3.1 PEGDA hydrogel properties

The swelling ratio is an important physical parameter defining permeability of hydrogels. For in vivo applications, swelling properties define the material allowance for nutrient/waste exchange. Swelling properties are also closely related to structural and mechanical properties. The mass swelling ratio is used to calculate polymer volume fraction in the swollen state - a parameter used to quantify average molecular weight between the crosslinks ($\overline{M_c}$). $\overline{M_c}$ determines mechanical strength of hydrogels (Lin et al., 2011). Hydrogels with high $\overline{M_c}$ values usually exhibit low compressive moduli but high ultimate strength. Hydrogel porosity is quantified through the mesh size parameter defined as an average linear distance between crosslinks (Koetting et al., 2015). Mesh size is a parameter that has been found to influence cell behavior. In the study by Lin et al. (2011), PEGDA hydrogels with larger mesh sizes have demonstrated increased chondrocyte proliferation rates, however, limited accumulation of ECM components.

These physical parameters can be controlled by varying the molecular weight of PEGDA precursor or by changing precursor concentration in polymerization solution. In this study, the latter approach was selected to investigate changes in physical properties. Variations in swelling, $\overline{M_c}$ and mesh sizes were chosen as ways to control drug release rates from PEGDA-PPy hydrogels.

The swelling ratios of PEGDA hydrogels with different PEGDA content are compared on fig. 3.3 (a). There was a statistically significant difference in SR values between samples with low PEGDA concentrations (20, 30, 40 and 50 % (w/v)). For example,

SR of PEGDA (20 %) was determined as 204±14 %, which is a double increase from the SR of PEGDA (40 %) 111±5 %. There was also a statistically significant difference between the low PEGDA concentration group of samples and hydrogels with high PEGDA concentrations (60, 70 and 80 % (w/v)), however, there was no significant difference in swelling ratios within the last group. Thus, PEGDA (60 %) had a SR value of 83±1 %, and PEGDA (80 %) an SR of 68±2 %. It is likely that within the sample group where PEGDA occupies more than a half of a material volume, changes in polymer concentration do not significantly contribute to the swelling properties. Moreover, swelling ratio values for this group of samples were $\leq$ 100 %. Similar trends have been observed for $\overline{M_c}$ and mesh size values, which are tabulated in table 3.1.

As expected, PEGDA (20 %) demonstrated the highest values for SR, $\overline{M_c}$ and mesh size parameters, therefore, this hydrogel should have the lowest compressive modulus but high permeability. PEGDA (40 %) hydrogel was selected to proceed with for the majority of experimental studies as it demonstrated good swelling and physical properties withing the group of hydrogels investigated. Given the statistically significant difference in swelling ratios between PEGDA 20, 40 and 80 % (w/v) (One-way ANOVA, F=10.19 , p=0.0049), these samples were selected for the study of controlled drug release.

As the drug release studies in this work are performed in a media with physiological pH values but also in alkaline media to stimulate release from PPy, it was necessary to first identify the swelling properties of PEGDA hydrogel in these media. Swelling ratios of PEGDA hydrogels in solutions with different pH values are presented on fig. 3.3. Hydrogel swelling greatly impacts the diffusion of the drug from the polymer. The swelling ratio of PEGDA (40 %) in pH 13 was significantly higher from SRs in other solutions: 373±41 % compared to 122±1 % in PBS and 171±13 % in pH 12 buffer solution (One-way ANOVA, F=88.48 , p=$9.18 \cdot 10^{-8}$). It has been reported that a slight increase in swelling ratios of PEGDA hydrogels can be seen in buffers with high pH values (Cavallo et al., 2017). This observation is linked to the hydrolytic degradation of PEGDA in

	MW between the crosslinks ($\overline{M_c}$)	Mesh size (ξ)
PEGDA content	Mean ±Standard deviation	Mean ±Standard deviation
20	67.03±9.35	0.79±0.07
40	55.58±4.13	0.64±0.03
60	54.65±1.12	0.61±0.08
80	55.27±2.17	0.59±0.01

Table 3.1: Average molecular weight between adjacent crosslinks and mesh sizes of PEGDA hydrogels with different concentrations of PEGDA (% (w/v)), calculated using the Peppas-Merrill model.

alkaline media (Browning et al., 2014; Browning and Cosgriff-Hernandez, 2012).

3.3.2 PEGDA-PPy characterization

Incorporation of PPy within the PEGDA hydrogels was achieved through the interfacial chemical polymerization method. Physical and structural properties of the composites were evaluated, firstly, to confirm the incorporation of PPy, and secondly, to explore the impact of PPy on PEGDA. Figure 3.4 demonstrates the FTIR spectra collected from PPy, PEGDA and PEGDA-PPy samples. It can be clearly seen that PEGDA-PPy spectra closely resembles PEGDA except for the band at 1565 cm^{-1}, which can be also found in the PPy spectra. This band is related to the vibration of single- and double- C–C bonds in the pyrrole ring, demonstrated on fig. 3.4 (b) (Tabaciarova et al., 2015). This confirmed the successful deposition of PPy on PEGDA hydrogels.

Swelling ratios of PEGDA-PPy were not significantly different compared to PEGDA. PEGDA(40 %)-PPy had a SR of 110±15 %, and PEGDA(80 %)-PPy SR was 67±14 %. These values are similar to SR values for PEGDA hydrogels, listed in section 3.3.1. Therefore, an incorporation of PPy did not impact the permeability of hydrogel matrix.

The results from conductivity measurements of PEGDA, PEGDA-PPy-a and PEGDA-PPy-b samples are presented in table 3.2. PEGDA hydrogels are non-conductive materials, and the deposition of PPy led to a significant increase in conductivity for

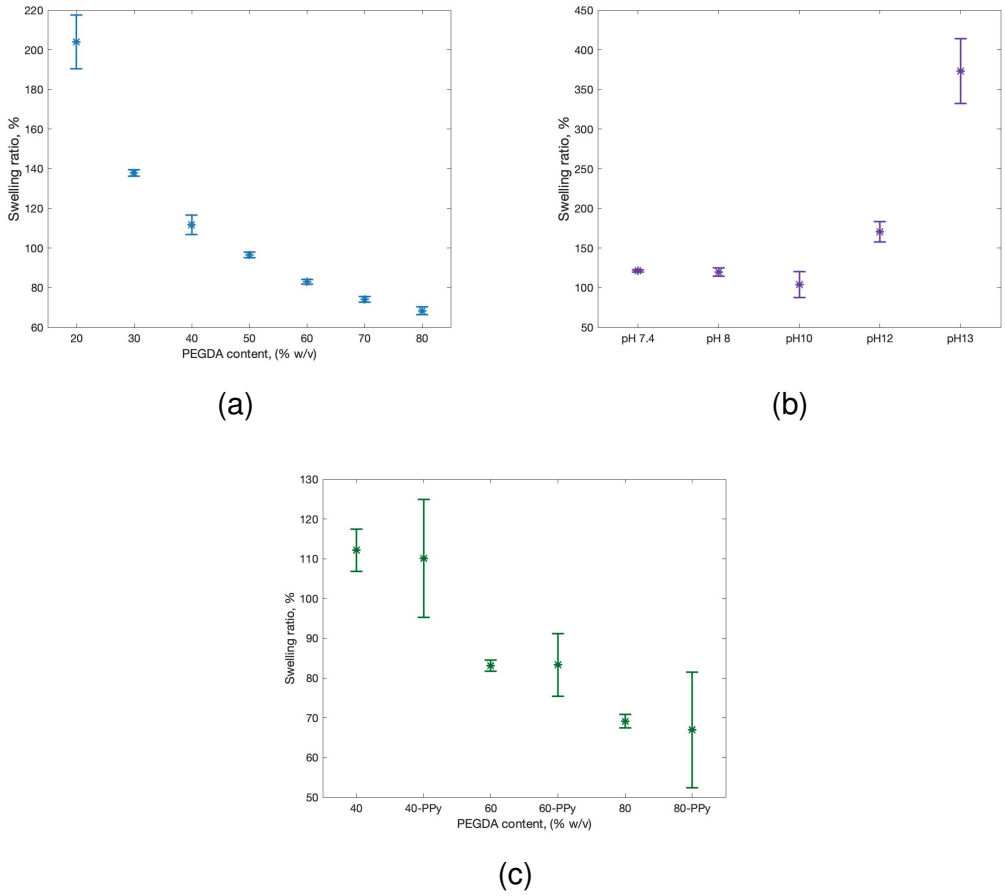

Figure 3.3: The swelling properties of PEGDA hydrogels depending on the PEGDA content (% (w/v)) (a), pH of the solution (b), deposition of PPy (c). Data points represent mean values ±standard deviation.

	Conductivity, $S \cdot cm^{-1}$
PEGDA	$(2.95 \pm 0.62) \cdot 10^{-11}$
PEGDA-PPy-a	$(3.70 \pm 0.15) \cdot 10^{-9}$
PEGDA-PPy-b	$(2.3 \pm 2.1) \cdot 10^{-4}$

Table 3.2: The average conductivity of PEGDA, PEGDA-PPy hydrogels prepared with standard (PEGDA-PPy-a) and modified (PEGDA-PPy-b) methods, data presented as mean value ±standard deviation.

PEGDA-PPy samples (unpaired t-test, $p \leq 0.0001$). Interestingly, there was also an increase in conductivity for PEGDA-PPy-b samples compared to PEGDA-PPy-a, however, it was not statistically significant (unpaired t-test, $p = 0.007$).

Cyclic voltammetry (CV) was performed on PEGDA-PPy samples prepared with two ICP methods. Graphs representing the first CV cycles for both materials are shown in fig. 3.5. When the potential is scanned from high (positive) values to low (negative), the reduction reaction occurs meaning the loss of electrons from PPy. Then the potential is increased and polymer is oxidized. It can be clearly seen that PEGDA-PPy-b sample demonstrates higher magnitude in reduction. This is likely due to the higher amounts of PPy being deposited on the surface of PEGDA-PPy-b compared to other samples. Increased surface area provides an increased number of doping sites, where electron exchange is more readily possible. This improved electrochemical performance of PEGDA-PPy samples prepared with modified ICP method is important for applications in sensors and actuators, and also for drug delivery. As previously mentioned in section 2.2.2, electrochemical doping is one of the most common methods used for drug incorporation with PPy. An improved electrochemical performance of PEGDA-PPy-b samples prepared with chemical methods and primary doped with oxidizer anions could allow for dedoping (reduction) in electrochemical cell followed by the doping (oxidation) with the drug dopant of choice.

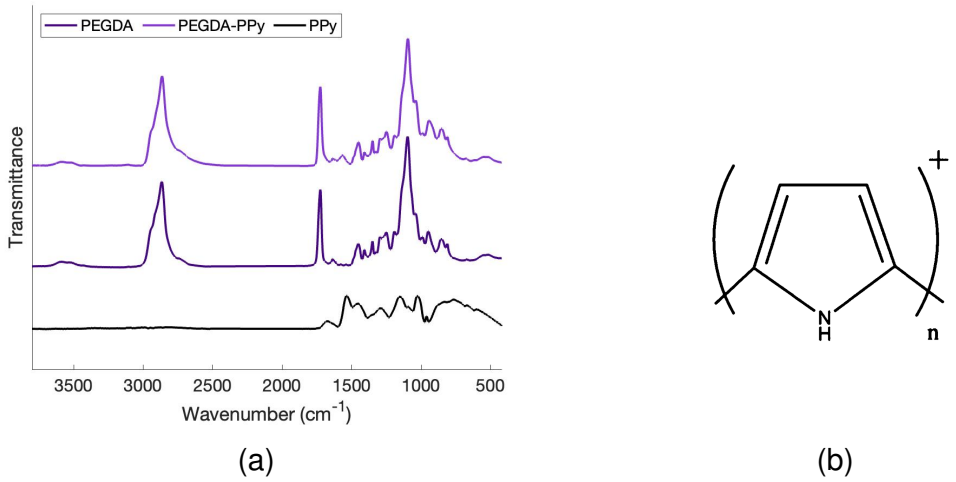

Figure 3.4: FTIR spectra of PEGDA, PPy and PEGDA-PPy (a). The band peak at 1565 cm^{-1} in PEGDA-PPy indicates a presence of double and single carbon bonds characteristic for pyrrole ring in the structure of PPy (b). © Gelmi et al. (2014), included with permission.

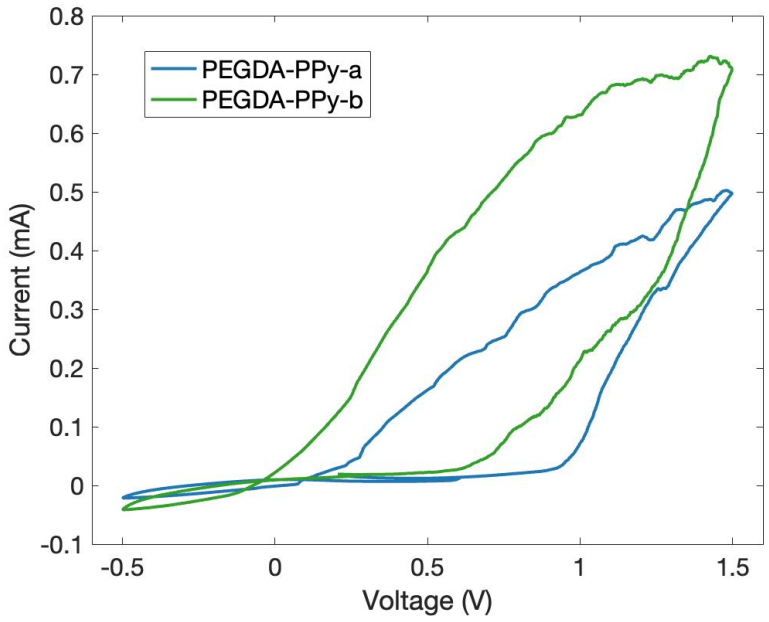

Figure 3.5: Cyclic voltammorgams of PEGDA-PPy-a and PEGDA-PPy-b demonstrating higher magnitude in reduction for PEGDA-PPy-b.

3.3.3 Surface morphology

As mentioned in section 3.2.2, changing the sequence of solutions for PEGDA immersion during interfacial chemical polymerization process yielded samples with different surface morphologies: PEGDA-PPy-a and PEGDA-PPy-b. These differences were first evaluated with optical microscopy and the pictures are presented on fig. 3.6. The surface of PEGDA-PPy-a looks smooth compared to PEGDA-PPy-b. The morphology of PEGDA-PPy-b indicates the presence of a rough PPy film covering the hydrogel. To further investigate surface structure of the composites, FESEM was performed. Microscopy pictures are presented on fig. 3.7. The typical globular *cauliflower* appearance of PPy can be seen in both PEGDA-PPy-a and PEGDA-PPy-b compared to the smooth PEGDA surface. PEGDA-PPy-b has large clusters of PPy polymer on the surface which are clearly charging when an electron beam from a microscope is applied. Overall, FESEM confirms optical microscopy findings and indicates that larger amount of PPy is accumulated on the surface of PEGDA-PPy-b. Improved electrochemical performance and higher conductivity of PEGDA-PPy-b discussed in section 3.3.2, therefore, can be explained by the high surface area.

The reason for the differences observed in surface morphologies is attributed to the method of preparation. For PEGDA-PPy-a materials, PEGDA is placed in an aqueous solution of oxidizer and then in the organic solution of pyrrole. PEGDA matrix swells very well in an aqueous media and adsorbs oxidizer in its structure. When the solution is changed to pyrrole, polymerization and PPy deposition preferentially occur within the structure of a hydrogel. In the case of PEGDA-PPy-b, the hydrogel is first placed in the organic solution of pyrrole, which does not penetrate the PEGDA pores as well as water, and therefore the pyrrole monomer accumulates within superficial layers. When the solution is changed to APS, nucleation sites for PPy polymerizaton occur primarily on the surface, leading to higher levels of polymer deposition within superficial layers.

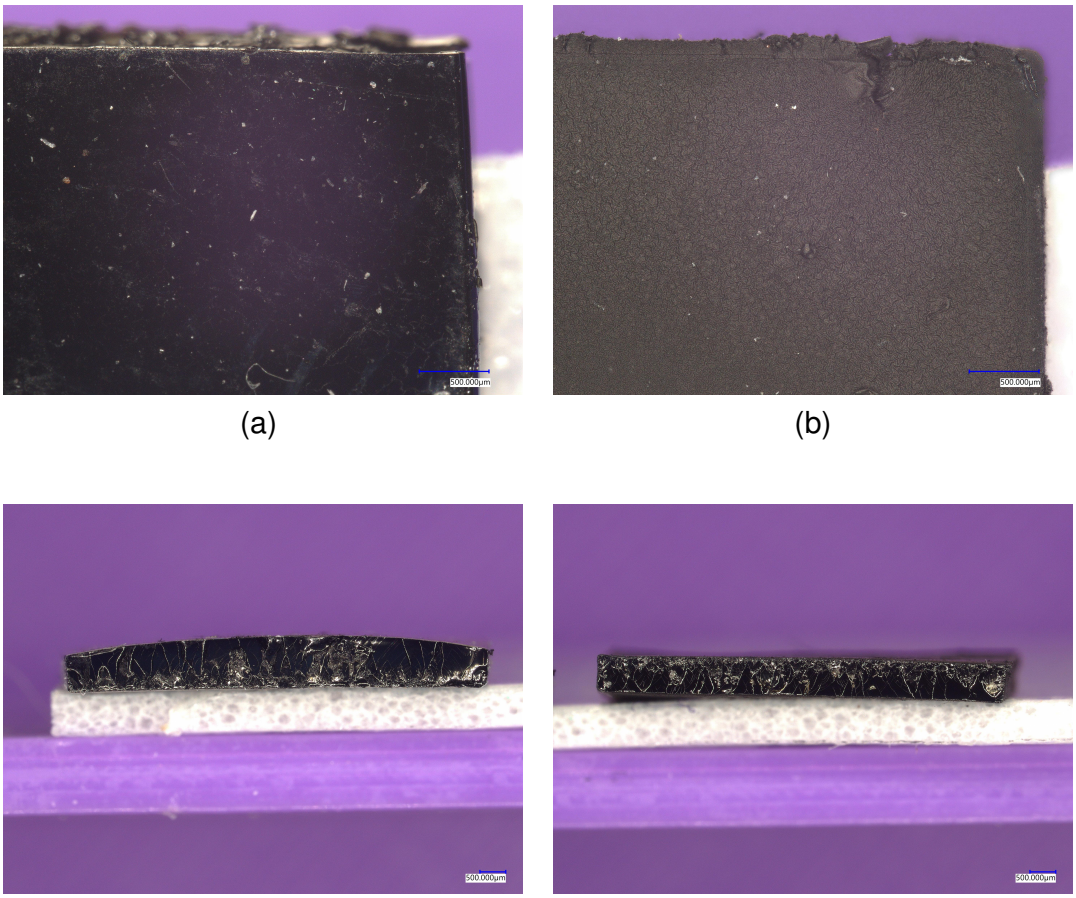

(a) (b)

(c) (d)

Figure 3.6: Optical microscopy pictures of PEGDA-PPy-a (a) and PEGDA-PPy-b (b) samples demonstrating variations in surface morphologies due to differences in fabrication methods. Cross-section images of PEGDA-PPy-a (c) and PEGDA-PPy-b (d) indicate that PPy has been sucessfully deposited through the thickness of PEGDA hydrogel using either of ICP methods. Scale bar represents 500 µm.

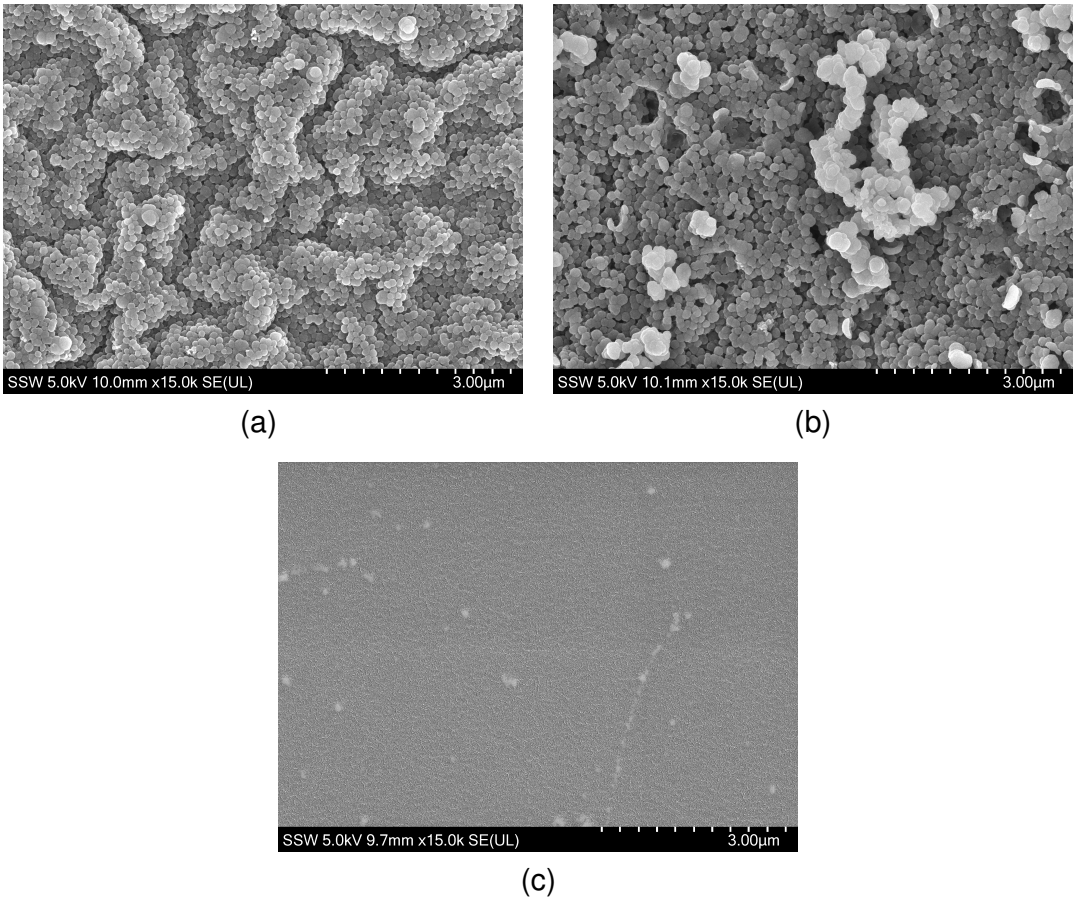

(a) (b)

(c)

Figure 3.7: Scanning electron microscopy pictures of PEGDA-PPy-a, demonstrating typical for PPy *cauliflower* surface morphology (a); PEGDA-PPy-b, demonstrating high amounts of deposited polymer (b); and PEGDA hydrogel with smooth unmodified surface (c).

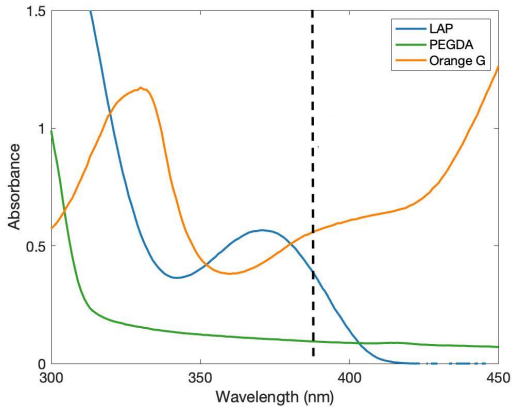

Figure 3.8: UV-absorbance of PEGDA resin components. The vertical line indicates printer emission wavelength $\lambda = 385\,\mathrm{nm}$.

3.3.4 3D printing

Previous studies on SLA and DLP 3D printing with PEGDA formulations have demonstrated the need for controlling the depth of light penetration in order to produce complex geometries and overhanging structures (Mau et al., 2019). An addition of UV-absorber is a common approach to reduce the depth of light penetration from the printer's light source. This allows the selective curing of the exposed layer of resin without simultaneous overcuring of the printed layers below, in addition to the realization of overhanging structures. Selection of the Orange G dye for the UV-absorber is motivated by the biocompatibility of the compound (Sinh et al., 2016).

As previously mentioned in section 3.2.3, the OMASML printer light source emission wavelength is 385 nm. From the fig. 3.8 it can be clearly seen that the absorbance of both LAP and Orange G dye at 385 nm is > 0, indicating the activity of the listed components at this wavelength.

Depth of cure tests were necessary to determine the optimal concentrations of LAP and UV-absorber in the formulation, and to select printing parameters. The results of the DoC test are presented in table 3.3. As expected, the DoC is decreasing with increasing concentrations of Orange G dye absorber. Additionally, there is an increase in DoC value

LAP, % (w/v)	UV-absorber, % (w/v)	Depth of cure, µm
0.05	0.5	93.1
	0.75	29.9
0.1	0.5	127.8
	0.75	61.3
	1	36.4

Table 3.3: The depth of cure values for PEGDA resin formulations containing different concentrations of PI (% (w/v)), and UV-absorber (% (w/v)).

for the 0.1 % (w/v) LAP resin formulations compared 0.05 % (w/v) LAP resin containing the same concentrations of the absorber. This finding can be explained by an increase in the speed of photopolymerization reaction due to higher concentrations of initiator.

A PEGDA resin formulation containing 0.1 % (w/v) LAP and 0.5 % (w/v) Orange G dye with a DoC value of 127.8 µm was selected for 3D printing. It is important to mention, that change of printing setup from DoC experiment to free surface printing fig. 3.1 (a) can slow down the rate of polymerization reaction during light exposure due to the consumption of free radicals generated by PI in oxygen. Therefore, the actual depth of cure value could decrease, and therefore the layer thickness printing parameter was prescribed as 100 µm.

Printing the DoC pattern (fig. 3.9(a)) using the conventional printer setup has demonstrated no overcuring in the XY-plane fig. 3.9 (b). Each printed layer can be visualized separately and layer thickness varied between 81 µm to 96 µm, which is attributed to the rapid drying and shrinkage of PEGDA. To demonstrate the ability to create overhanging structures using the selected resin formulation, a thin film was printed across the span of two supporting structures fig. 3.9 (c).

Resin printing resolution was explored through printing pillar structures of different diameters fig. 3.10 (a). It can be clearly seen on fig. 3.10 (b) that it was only possible to print pillars with diameters $>$ 400 µm. Only one layer of smaller diameter pillars (250 µm, 300 µm and 350 µm) could be printed. This is likely due to the insufficient stiffness of

the PEGDA 40 % (w/v) resin formulation. However, achieved resolutions are sufficient for tissue engineering applications.

In light of these results, a pillar diameter of 500 µm was selected for printing of tissue engineering scaffold models. This pillar pattern was printed with a 500 µm distance between pillars, shown on fig. 3.10 (c), to demonstrate that this distance allows for a sufficient outflow of liquid resin when the vat moves up and down in between the layers. Resin entrapment between the structures could lead to overcuring. Additionally, printing the two-layer film on top of the pillars was also successful, thus creating a basis structure for the tissue engineering scaffold model fig. 3.10 (d).

A tissue engineering scaffold model was created using the nTopology software fig. 3.11 (a–b) and represented the array of 500 µm pillars evenly spaced (500 µm) and connected together with a lattice structure at the base, middle and at the top. Distances between support lattice structures were also 500 µm, yielding a final pore size of 500 µm×500 µm. An optical micrograph of the porous PEGDA scaffold is presented in fig. 3.11 (c). Pore size measurements were performed in both the swollen (directly after printing) and dry states. In the swollen state the horizontal distance between the pillars varied between 603 µm to 607 µm, and 450 µm to 495 µm vertically. In the dried state these dimensions were 560 µm to 605 µm and 450 µm to 479 µm respectively. This structure was used for the interfacial chemical polymerization of pyrrole, yielding the PEGDA-PPy scaffold presented in fig. 3.11 (d). Print dimensions have been preserved after the deposition of PPy.

Biomaterial scaffolds are responsible for structural support and integrity of the TE complex, and they also have to provide enough space for the formation and growth of new tissue. The *gold standard* is that the material occupies $\approx$ 25 % of the structure volume, while $\approx$ 75 % is left *open* (Aisenbrey et al., 2018). In order to achieve these parameters with the PEGDA formulation, the stiffness issue can be addressed through increasing PEGDA concentration and varying LAP and UV-absorber content accordingly.

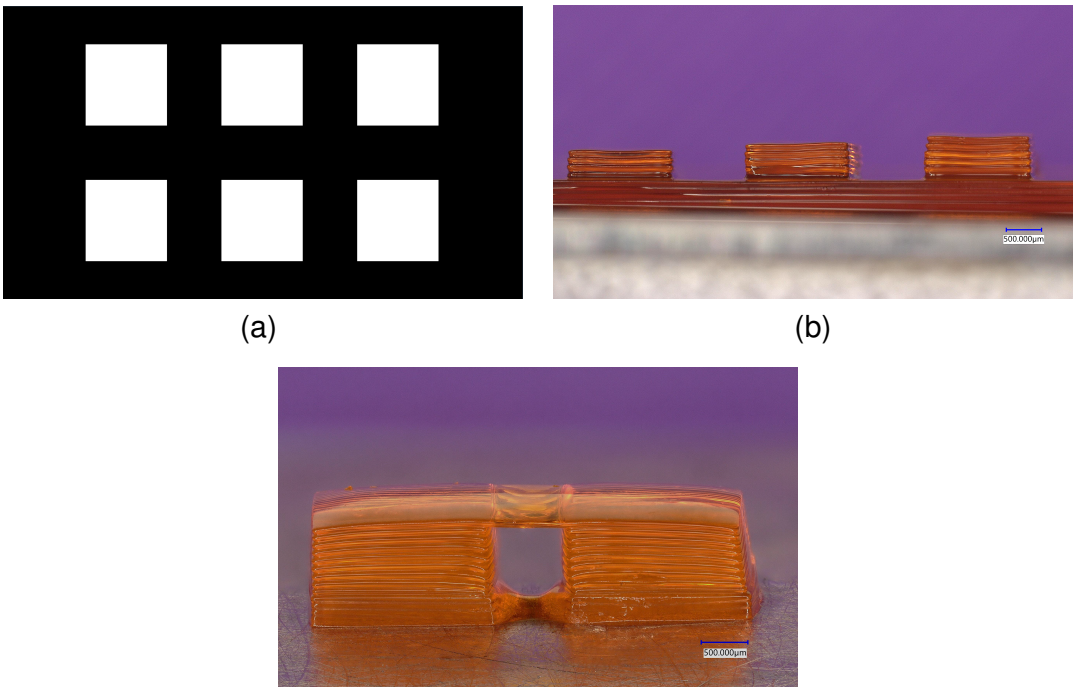

(a) (b)

(c)

Figure 3.9: Pattern used for the DoC tests where features in white are being projected as images (a); 3D print testing the layer printing height based on the DoC pattern (b); 3D print testing printing of overhanging structures (c). Scale bar represents 500 µm.

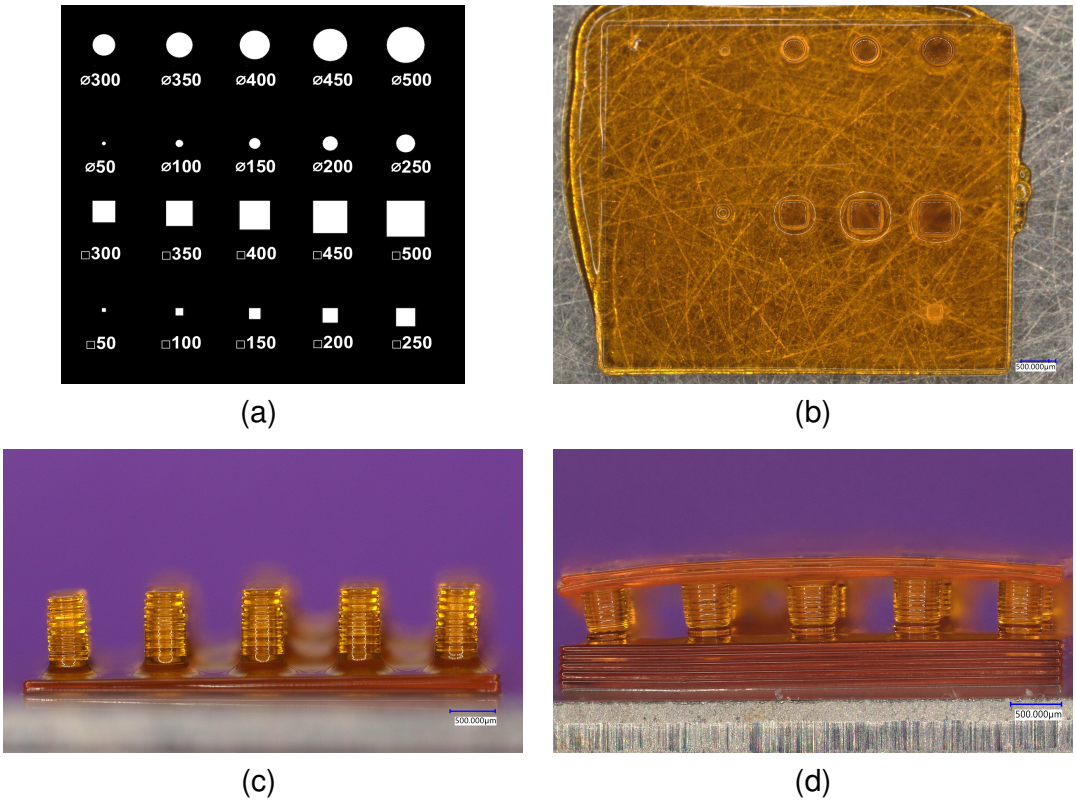

Figure 3.10: Pillar pattern used for the resolution test (a); printed pillar resolution test pattern (b); the array of pillars 500 µm in diameter printed on a 2-layer base film (c); the array of pillars 500 µm in diameter printed in a 6-layer base film with a 2-layer film printed on top (d). Scale bar represents 500 µm.

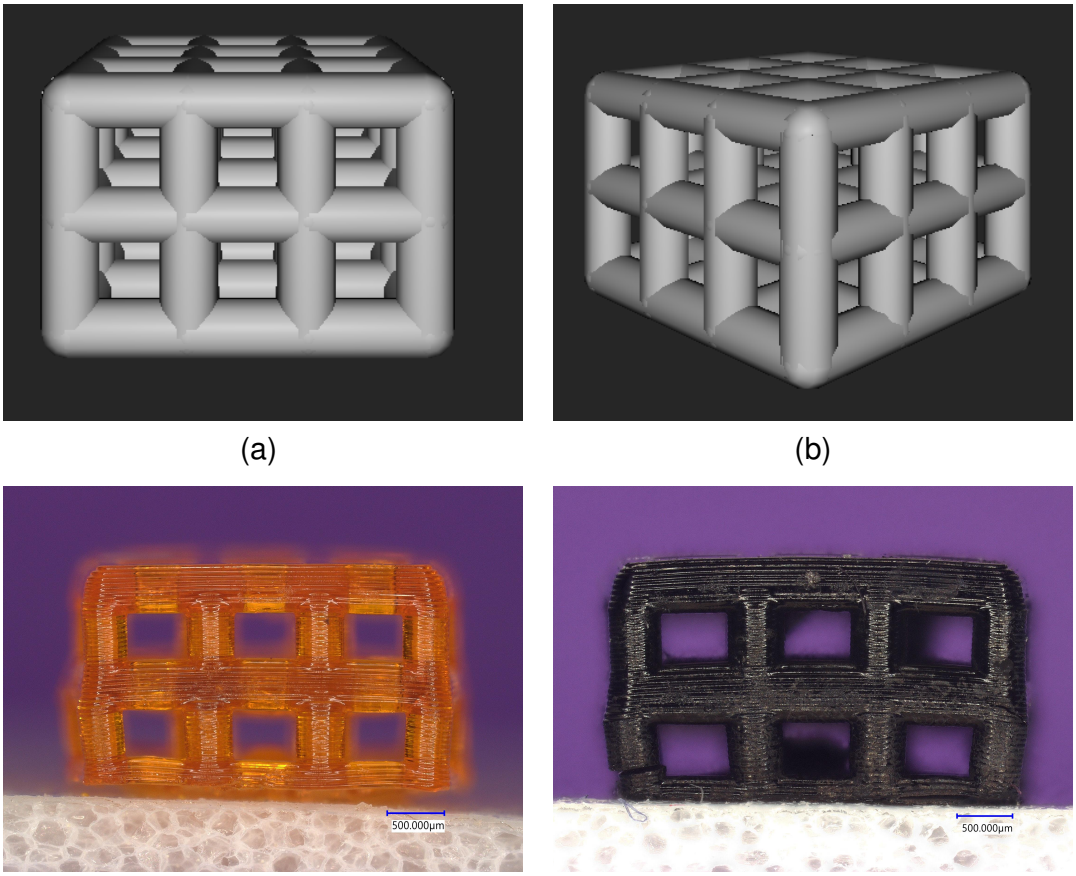

Figure 3.11: The model of a lattice structure created using nTopology software (a-b); PEGDA lattice 3D-printed as a tissue engineering scaffold model (c); PEGDA-PPy scaffold created after PPy deposition on to the previous PEGDA structure using the ICP method. Scale bar represents 500 µm.

3.4 Chapter summary

This chapter described the fabrication process for composite conducting PEGDA-PPy hydrogels. A photopolymerization reaction was implemented to prepare a PEGDA hydrogel matrix used for the deposition of PPy via interfacial chemical oxidative polymerization. Structural and physical properties of PEGDA and PEGDA-PPy were then investigated. Lastly, 3D printing capabilities of PEGDA resin using the custom-designed OMASML DLP printer were discussed. The results presented in this chapter establish that this methodology for the creation of electoactive conducting PEGDA-PPy tissue engineering scaffolds is viable.

3.5 List of references

Aisenbrey, E. A., Tomaschke, A., Kleinjan, E., Muralidharan, A., Pascual-Garrido, C., McLeod, R. R., Ferguson, V. L. and Bryant, S. J. (2018), 'A stereolithography-based 3D printed hybrid scaffold for in situ cartilage defect repair', *Macromolecular Bioscience* **18**(2), 1700267.

Browning, M. B., Cereceres, S. N., Luong, P. T. and Cosgriff-Hernandez, E. M. (2014), 'Determination of the in vivo degradation mechanism of PEGDA hydrogels', *Journal of Biomedical Materials Research Part A* **102**(12), 4244–4251.

Browning, M. B. and Cosgriff-Hernandez, E. (2012), 'Development of a biostable replacement for PEGDA hydrogels', *Biomacromolecules* **13**(3), 779–786.

Cavallo, A., Madaghiele, M., Masullo, U., Lionetto, M. G. and Sannino, A. (2017), 'Photocrosslinked poly(ethylene glycol) diacrylate (PEGDA) hydrogels from low molecular weight prepolymer: Swelling and permeation studies', *Journal of Applied Polymer Science* **134**(2), 44380.

Choi, J. R., Yong, K. W., Choi, J. Y. and Cowie, A. C. (2019), 'Recent advances in photo-crosslinkable hydrogels for biomedical applications', *BioTechniques* **66**(1), 40–53.

Cullen, A. T. and Price, A. D. (2018), 'Digital light processing for the fabrication of 3D intrinsically conductive polymer structures', *Synthetic Metals* **235**, 34–41.

Cullen, A. T. and Price, A. D. (2019), 'Fabrication of 3D conjugated polymer structures via vat polymerization additive manufacturing', *Smart Materials and Structures* **28**(10), 104007.

Fedorovich, N. E., Oudshoorn, M. H., van Geemen, D., Hennink, W. E., Alblas, J. and Dhert, W. J. (2009), 'The effect of photopolymerization on stem cells embedded in hydrogels', *Biomaterials* **30**(3), 344–353.

Gelmi, A., Ljunggren, M. K., Rafat, M. and Jager, E. W. (2014), 'Influence of conductive polymer doping on the viability of cardiac progenitor cells', *Journal of Materials Chemistry B* **2**(24), 3860–3867.

Holness, F. B., Guillén, G. P. and Price, A. D. (2021), Hierarchical electroactive polypyrrole-carbon nanotube composite microstructures by high resolution vat polymerization and soft template electropolymerization, *in* 'Electroactive Polymer Actuators and Devices (EAPAD) XXIII', Vol. 11587, SPIE, pp. 103–110.

Koetting, M. C., Peters, J. T., Steichen, S. D. and Peppas, N. A. (2015), 'Stimulus-responsive hydrogels: Theory, modern advances, and applications', *Materials Science and Engineering R: Reports* **93**, 1–49.

Lawrence, M. (2021), '3D printed polypyrrole scaffolds for pH dependent drug delivery with applications in bone regeneration', *The University of Western Ontario Electronic Thesis and Dissertation Repository* **7837**.

Lee, K. Y., Rowley, J. A., Eiselt, P., Moy, E. M., Bouhadir, K. H. and Mooney, D. J. (2000), 'Controlling mechanical and swelling properties of alginate hydrogels independently by cross-linker type and cross-linking density', *Macromolecules* **33**(11), 4291–4294.

Lin, S., Sangaj, N., Razafiarison, T., Zhang, C. and Varghese, S. (2011), 'Influence of physical properties of biomaterials on cellular behavior', *Pharmaceutical Research* **28**(6), 1422–1430.

Mau, R., Nazir, J., John, S. and Seitz, H. (2019), 'Preliminary study on 3D printing of PEGDA hydrogels for frontal sinus implants using digital light processing (DLP)', *Current Directions in Biomedical Engineering* **5**(1), 249–252.

Samanta, D., Meiser, J. L. and Zare, R. N. (2015), 'Polypyrrole nanoparticles for tunable, pH-sensitive and sustained drug release', *Nanoscale* **7**(21), 9497–9504.

Sinh, L. H., Harri, K., Marjo, L., Minna, M., Luong, N. D., Jürgen, W., Torsten, W., Matthias, S. and Jukka, S. (2016), 'Novel photo-curable polyurethane resin for stereolithography', *RSC Advances* **6**(56), 50706–50709.

Tabaciarova, J., Mičušík, M., Fedorko, P. and Omastová, M. (2015), 'Study of polypyrrole aging by xps, ftir and conductivity measurements', *Polymer Degradation and Stability* **120**, 392–401.

Taha, M. H. F., Ashraf, H. and Caesarendra, W. (2020), 'A brief description of cyclic voltammetry transducer-based non-enzymatic glucose biosensor using synthesized graphene electrodes', *Applied System Innovation 2020, Vol. 3, Page 32* **3**(3), 32.

Uttayarat, P., Boonsirichai, K., Tangthong, T., Pimton, P., Thongbopit, S. and Phermthai, T. (2016), Photopolymerization of hydrogels for cartilage tissue engineering, Institute of Electrical and Electronics Engineers Inc.

Chapter 4

Drug Incorporation and Delivery from the Composite PEGDA-PPy Hydrogels

This chapter explores the drug delivery capabilities of composite PEGDA-PPy hydrogels. Doping of anionic compounds with PPy during chemical oxidative polymerization is discussed. Drug release was performed in Phosphate Buffer Saline solution with physiologically relevant pH and in alkaline media to facilitate the expulsion of the drug from the PPy component. Control over the drug release rates was achieved through variations in PEGDA matrix density and is presented in this chapter.

4.1 Introduction

Conducting polymers have been extensively investigated as potential candidates for localized drug delivery applications (Tandon et al., 2018). The interest in using PPy for drug delivery comes mainly from the electroactivity of the polymer. The ability of PPy to change its structural (doping/de-doping with ionic compounds) and physical (shape, volume) properties in a response to electrical stimuli was recognised as a promising strategy for drug release or biological sensor applications.

Section 2.2.2 outlines mechanisms involved in drug loading and release from CPs, namely PPy. The majority of studies exploring CPs for drug delivery applications rely on the doping performed through electrochemical oxidation/reduction of the polymer (Tandon et al., 2018). During chemical oxidative polymerization, incorporation of a dopant is possible, however, is usually limited to small anionic species coming from the oxidizer (Wallace et al., 2002). This chapter aims to explore doping of PPy with anionic compounds during chemical oxidative polymerization, and possible limitations associated with this process.

Although electrical stimulation has been very effective in delivering doped drugs from PPy in the experimental setup (Uppalapati et al., 2016), there is an ongoing search for a feasible in vivo release stimulus. Samanta et al. (2015) have performed a study on drug delivery from PPy NPs stimulated by changes in pH of the environment. Deprotonation reaction of PPy in the alkaline media, briefly described in section 2.2.2, caused expulsion of the doped drug. Samanta et al. (2015) also describe successful dopant release at physiological pH values (7.4). Lawrence (2021) has also demonstrated dopant release from PPy NPs over the physiological pH range (6 to 8). In this chapter, alkaline media (pH 11.2) was used to trigger release of a drug from PEGDA-PPy hydrogels to confirm dopant incorporation. Release of the dopant from PEGDA-PPy in the Phosphate Buffer Saline (pH 7.4) was also investigated.

4.2 Materials and Methods

To demonstrate the potential of PPy to perform as a drug carrier in composite PEGDA-PPy hydrogels, PPy was doped with a model anionic compound, Fluorescein sodium salt (Fl) (CAS #2321-07-5). The doping process was performed during the interfacial chemical polymerization described in section 3.2.2. Fl (0.04 mol) was dissolved in an aqueous solution of the oxidizer, APS. Oxidizer molarity was reduced to 0.1 mol

to facilitate the doping of PPy with Fl. Dried PEGDA hydrogels were placed in the oxidizer-dopant solution for 2 h and then transferred in to the solution of pyrrole (0.1 mol) in cyclohexane. After polymerization was completed, PEGDA-PPy-Fl samples were gently rinsed with ethanol and left to dry overnight. The pH of the solutions employed for the polymerization and doping were monitored with the Mettler Toledo benchtop pH-meter throughout the process.

Two control groups of samples: PEGDA-Fl and PPy-Fl were prepared to study the release of Fl separately from the PEGDA matrix and the polymer PPy. For PEGDA-Fl, PEGDA hydrogels were soaked in an aqueous solution of Fl for 2 h, rinsed with distilled water and dried overnight. PPy powder doped with Fl was prepared using the methodology described in section 3.2.2. An aqueous solution of APS 0.1 mol and Fl (0.14 mol) was mixed with 0.1 mol of pyrrole in cyclohexane resulting in the precipitation of CP particles. The particles were paper-filtrated from the polymerization mixture, quickly rinsed with ethanol and dried overnight prior to the experiments. All samples were protected from the light after preparation and during release studies. Both PEGDA-Fl and PEGDA-PPy-Fl hydrogels had an equal surface area of 2.7 cm^2.

Drug release studies were conducted in Phosphate Buffer Saline (PBS, pH 7.4) and in 0.01 mol aqueous solution of NaOH (pH 11.2). Experimental (PEGDA-PPy-Fl) and control samples (PEGDA-Fl or PPy-Fl) were placed in 3 mL of the release media. The mass of PPy-Fl for release studies was measured as 0.08 g. Absorbance data from release media was collected using a Cary 60 UV-vis spectrometer at 2 h of release. Fl concentrations in release solutions for each sample were calculated using the collected absorbance data and standard curve method. Fl has a pH-sensitive maximum absorbance value Guern et al. (2020), therefore, separate standard curves were prepared for Fl in PBS and NaOH solutions.

For the controlled drug delivery experiment, PEGDA hydrogels with PEGDA concentrations of 20 % (w/v), 40 % (w/v) and 80 % (w/v) were prepared for PPy deposition to

explore the influence of the hydrogel matrix density on Fl release rates. PPy polymerization was performed as previously outlined. Release studies were performed using the 0.01 mol NaOH solution (pH 11.2). Each sample was placed in 5 mL of release media, and 20 µL of the media was drawn every 30 min over a span of 8 h. The total decrease in the release media volume by the final time-point was 2.4 % and was considered negligible. A media sample was dissolved in 1 mL NaOH solution for UV spectrometry. Fl concentrations were back-calculated using the standard curve method.

All data was collected in triplicates (n=3), unless stated otherwise, to calculate average values and standard deviations (±). One- or two-way analysis of variance (ANOVA) and multiple comparison test were performed in MATLAB.

4.3 Results and Discussion

4.3.1 Drug doping with PPy during chemical polymerization

During chemical oxidative polymerization of PPy, small anions arising from oxidizer (for example, persulfate anions in the case of APS), could be doped with PPy much easier than any other added anionic compounds (Wallace et al., 2002). Also, an addition of oxidizer could impact the structural properties of Fl. These factors were explored and are reported below.

Following the steps of doping with Fl during chemical oxidative polymerization, PEGDA matrix was subsequently submerged in aqueous solution of oxidizer with Fl, and then in cyclohexane containing pyrrole monomer. The mole ratio of the dopant:pyrrole was 0.4:1, and oxidizer:pyrrole ratio was 1:1. According to Wallace et al. (2002), the ideal oxidizer:pyrrole ratio is 1.3:1 for two-electron oxidizers (e.g. APS) to allow the two electrons provided by the oxidizer to efficiently incorporate pyrrole monomers within the polymer. Every 3rd or 4th pyrrole unit is then doped with an anion for electrochemical neutrality. For drug doping, the oxidizer concentration was reduced to prevent the

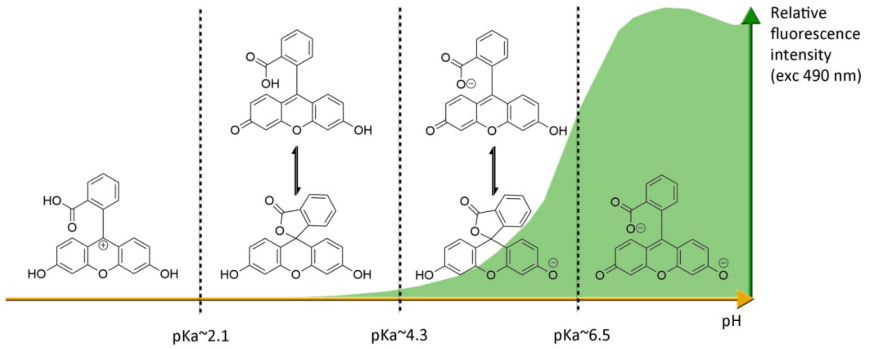

Figure 4.1: Ionic forms of Fl depending on the pH of the environment. Di-anionic form of Fl existing at neutral pH levels and giving the maximum absorbance at 490 nm is transforming into mono-anionic and further into neutral and cationic forms with a progressive acidification of the environment. This is followed by the decrease in fluorescence and maximum absorbance peak shifting to the left. (© Guern et al. (2020) included with permission)

competitive incorporation of persulfate ions along with Fl.

The pH of Fl/APS solution was found to be 2.7. According to Guern et al. (2020), acidification of the solution can lead to the transformation of anionic form of Fl into the neutral or cationic form (fig. 4.1). As previously described in section 2.2.1, PPy doping implies incorporation of anionic species into the polymer chain to balance out an excessive positive charge of as-synthesized PPy (Tandon et al., 2018). Cationic and neutral forms of Fl are unlikely to act as counter ion dopants for PPy. However, in the chemical doping process used in this study, change of solution to pyrrole/cyclohexane with a pH of 7.7 was done to reverse this effect.

For drug delivery studies, alkaline pH media was used as a release stimulus. PPy in alkaline media undergoes a deprotonation reaction specific for this polymer. As previously described in section 2.2.2, PPy has an excessive amount of hydrogen ions, which are linked with anionic dopants to maintain the stability of the polymer backbone. When the polymer is placed in the environment with low hydrogen ion concentration (high pH), it causes the expulsion of H^+ from the backbone, along with the dopants (Samanta et al., 2015). Therefore, an increase in Fl release rates from PPy and PEGDA-PPy in alkaline solution would indicate that Fl performed as a dopant.

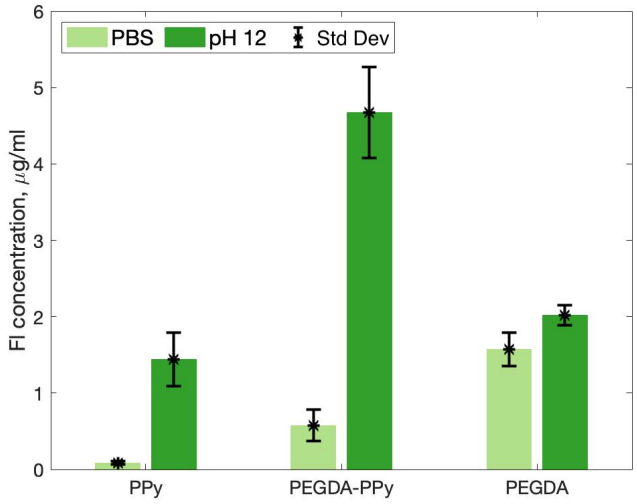

Figure 4.2: 2 h Fl release from PPy, PEGDA-PPy and PEGDA hydrogels in PBS and NaOH solution (pH 11.2). Higher release rates in alkaline media can be seen for all samples, indicating deprotonation reaction of PPy causing the expulsion of a dopant, and increased swelling of PEGDA in high pH media.

Alkaline media (pH 11.2) caused significant differences in Fl release rates compared to release in PBS for all three sample groups, and yielded significantly different results between control and experimental sample groups as well (pH 7.45), (Two-way ANOVA, F=179.4, $p=1.4\cdot10^{-8}$) as shown in fig. 4.2. PEGDA-PPy samples released only 0.57±0.20 µg · mL^{-1} of Fl in PBS, but 4.67±0.59 µg · mL^{-1} in NaOH solution. It was also seen that Fl release rates for PEGDA hydrogels were slightly higher in the NaOH solution compared to PBS: 2.02±0.13 µg · mL^{-1} and 1.58±0.21 µg · mL^{-1} respectively. This can be explained by the increased rate of swelling of PEGDA in alkaline solutions previously described in section 3.3.1. Although, increased rate of PEGDA swelling might contribute to higher rates of Fl release in PEGDA-PPy samples, overall, PEGDA-PPy samples released statistically significantly higher Fl amounts in alkaline media than PEGDA samples (One-way ANOVA, F=79.78, $p=8.76\cdot10^{-9}$). This significant difference indicates the deprotonation reaction of PPy and proves an incorporation of Fl in PPy as a dopant. Additionally, drug delivery performance of PPy fabricated and doped with Fl

using the same chemical oxidative polymerization method confirms these findings.

The absorbance values collected at 490 nm from the PPy-Fl samples were in the negative range: −0.024 to −0.028, indicating the absence of Fl. In contrast, the absorbance values collected from NaOH solution were ranging between 0.207 to 0.328, yielding the average Fl concentration released from PPy to be $1.43 \pm 0.35\,\mu g \cdot mL^{-1}$. Physiological pH values do not cause deprotonation of the polymer. According to Pei and Qian (1991), the pK_a value for the deprotonation of PPy is in the range of 9 to 11. Given this, it is unlikely that PPy will release anionic dopants in physiological media without external stimulation. However, PEGDA-PPy hydrogels have demonstrated low Fl release levels in PBS likely contributed by the diffusion of undoped Fl from PEGDA matrix. For drug delivery purposes, PEGDA-PPy hydrogels can provide the immediate dose of the drug through the diffusion from PEGDA matrix, followed by the delivery of higher doses from stimulated PPy.

Given the infeasibility of alkaline pH stimuli for the delivery of anionic drugs from PPy in vivo, other triggers need to be investigated. External electrical stimulation causing reduction of the polymer and dopant release is theoretically possible, however, has not yet been studied in vivo. Another promising external stimuli for drug release from PPy is a near-infrared(NIR) radiation. In the study by Tiwari et al. (2018) the NIR laser exposure has caused the delivery of anti-tumour drug paclitaxel (PTX) from PPy-coated polycaprolactone fibers.

Low acidic pH values are more common in vivo. For example, gastric juice has a pH value ranging from 1.0 to 3.0, or inflammation can lower the pH of the tissues (5.4 to 7.4) (Koetting et al., 2015). According to Samanta et al. (2015), release of positively-charged drugs is possible from PPy in the acidic media via protonation reaction of the polymer (section 2.2.2). Therefore, investigating the incorporation of positively charged drugs into PPy, and their release in acidic media is advised for future research.

4.3.2 Controlled drug release from PEGDA-PPy hydrogels

Additional control over the rates of Fl release from PPy was achieved through variations in PEGDA matrix density. The results of this experiment are presented in fig. 4.3. PEGDA-PPy hydrogels with PEGDA content of 20, 40 and 80% were selected for this study based on the statistically significant differences in swelling ratios discussed in section 3.3.1. Overall, the set of samples used for this experiment achieved significantly higher Fl release rates than samples used in the previous tests.

It can be clearly seen that PEGDA(20 %)-PPy hydrogels demonstrated the fastest rate of Fl accumulation due to the lowest matix density. For example, the 2 h Fl release concentration for PEGDA(20 %)-PPy was 35.40±0.68 mg · mL^{-1}, what was significantly higher than the Fl concentrations of 23.62±1.65 mg · mL^{-1} and 27.39±0.98 mg · mL^{-1} for PEGDA(40 %)-PPy and PEGDA(80 %)-PPy hydrogels respectively (One-way ANOVA, F=78.71, p=4.94·10^{-5}). The speed of Fl accumulation during the first 2 h of release (the difference between 2 h and 30 min Fl amounts) was statistically significant between PEGDA(20 %)-PPy and two other sets of samples (One-way ANOVA, F=75.38, p=5.6·10^{-5}), but not between the latter. Thus, the amount of Fl accumulated from PEGDA(20 %)-PPy was 17.26±0.50 mg · mL^{-1}, while for PEGDA(40 %)-PPy it was only 8.14±1.48 mg · mL^{-1}. Interestingly, over the next 6 h, Fl release speed from PEGDA(40 %)-PPy was significantly higher (21.30±0.36 mg · mL^{-1}), while PEGDA(20 %)-PPy demonstrated the lowest rate of Fl accumulation (15.16±1.40 mg · mL^{-1}; One-way ANOVA, F=39.14, p=0.0004).

PEGDA(80 %)-PPy samples overall showed similar to PEGDA(40 %)-PPy trends for Fl release speed: only 9.48±0.65 mg · mL^{-1} for the first 2 h and 17.90±0.33 mg · mL^{-1} for the following 6 h. Although, as previously mentioned, the 2 h Fl amounts were statistically higher for PEGDA(80 %)-PPy than for PEGDA(40 %)-PPy.

The 24 h Fl release amounts were statistically significant between PEGDA(80 %)-PPy and PEGDA(40 %)-PPy & PEGDA(20 %)-PPy (One-way ANOVA, F=71.06, p=6.65·10^{-5}).

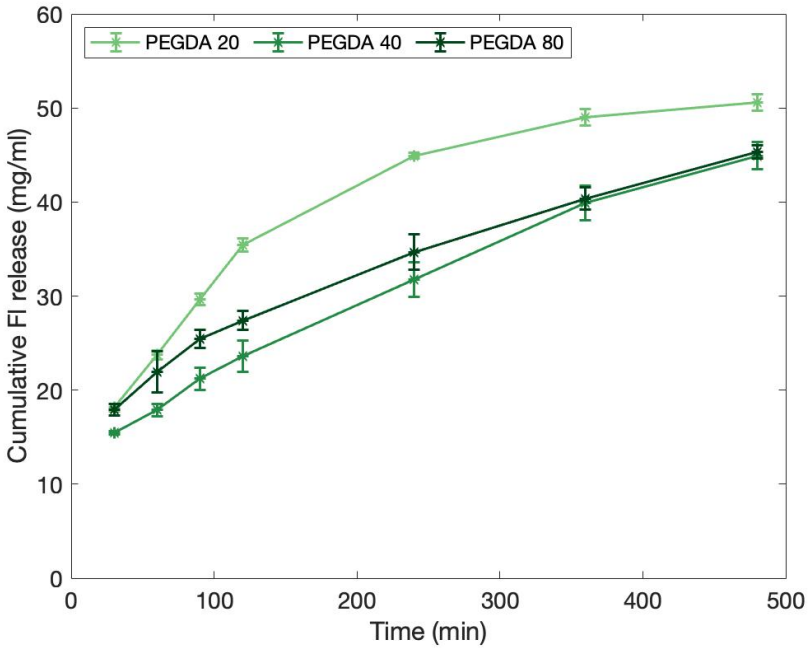

Figure 4.3: FI release from PEGDA(20 %)-PPy, PEGDA(40 %)-PPy and PEGDA(80 %)-PPy, data collected over a span of 8 h with 30 min increments. PEGDA(20 %-PPy demonstrates the fastest release rate due to the low hydrogel density allowing for easy drug diffusion. Data points represent meaan values ±standard deviation.

Final release values are presented in table 4.1. Higher final amount of FI released from PEGDA(80 %)-PPy could indicate the higher FI loading for 80 % sample. Additionally, there was a significant difference between 8 h and 24 h FI release values for PEGDA(40 %)-PPy and PEGDA(80 %)-PPy samples (One-way ANOVA, F=120.86, $p=7.79 \cdot 10^{-10}$), but no significant difference was seen for PEGDA(20 %)-PPy. This means that PEGDA-PPy hydrogels will allow for more gradual release of the drug.

An approach of controlling drug release rate from hydrogels by tuning the matrix density has been previously described in the study by Shirakura et al. (2017). There, hydrogel NPs with loose matrix have demonstrated a faster rate of drug release over 75 h period. In the new study by Briggs et al. (2022), polyacrilamide hydrogel matrix density was increased using two different approaches: by adding higher amounts of polymer, and through increasing concentrations of the crosslinker. In both cases, reduced

24 h Fl release	
Sample	Fl concentration ($mg \cdot mL^{-1}$)
PEGDA(20%)-PPy	55.49±1.37
PEGDA(40%)-PPy	52.72±1.31
PEGDA(80%)-PPy	63.25±0.41

Table 4.1: Fl release values collected from PEGDA(20 %)-PPy, PEGDA(40 %)-PPy and PEGDA(80 %)-PPy hydrogels at 24 h presented as mean values ±standard deviation

drug release rates were demonstrated associated with higher hydrogel crosslinking density, regardless of the intitial drug loading. In the case of composite CHs, hydrogel matrix mitigates the initial burst release of drug from the PPy. For example, in the work by Samanta et al. (2015), PPy NPs were dispersed in calcium alginate hydrogel for the sustained release of piroxicam. The long-term delivery study from hydrogel demonstrated a much slower rate of piroxicam accumulation compared to NPs.

As previously discussed in section 3.3.1, PEGDA(20 %) had significantly higher swelling ratio and mesh size than PEGDA(40 %) and PEGDA(80 %). This is first to our knowledge study investigating the relationship between PEGDA crosslink density and drug release rates from PPy incorporated into hydrogel matrix. Low matrix density and higher distance between the polymer chains in PEGDA(20 %) facilitates the permeability of hydrogel and diffusion of Fl released from PPy deposited within the matrix. By varying PEGDA hydrogel matrix density, different levels of control over release rate could be achieved for PEGDA-PPy materials.

4.4 Chapter summary

This chapter has demonstrated successful doping of PPy with anionic compound Fl via oxidative chemical polymerization. Drug release from PEGDA-PPy was initiated in solutions with alkaline and physiological pH values. This chapter describes stimulation of dopant release in relation to in vivo applications. Control over drug delivery rates

was achieved through varying concentrations of PEGDA precursor leading to different matrix densities of PEGDA-PPy material. These results have demonstrated the viability of PEGDA-PPy materials for sustained drug delivery and unlock new research directions for various types of dopant molecules and release triggers.

4.5 List of references

Briggs, F., Browne, D. and Asuri, P. (2022), 'Role of polymer concentration and crosslinking density on release rates of small molecule drugs', *International Journal of Molecular Sciences 2022, Vol. 23, Page 4118* **23**(8), 4118.

Guern, F. L., Mussard, V., Gaucher, A., Rottman, M. and Prim, D. (2020), 'Fluorescein derivatives as fluorescent probes for pH monitoring along recent biological applications', *International Journal of Molecular Sciences 2020, Vol. 21, Page 9217* **21**(23), 9217.

Koetting, M. C., Peters, J. T., Steichen, S. D. and Peppas, N. A. (2015), 'Stimulus-responsive hydrogels: Theory, modern advances, and applications', *Materials Science and Engineering R: Reports* **93**, 1–49.

Lawrence, M. (2021), '3D printed polypyrrole scaffolds for pH dependent drug delivery with applications in bone regeneration', *The University of Western Ontario Electronic Thesis and Dissertation Repository* **7837**.

Pei, Q. and Qian, R. (1991), 'Protonation and deprotonation of polypyrrole chain in aqueous solutions', *Synthetic Metals* **45**(1), 35–48.

Samanta, D., Meiser, J. L. and Zare, R. N. (2015), 'Polypyrrole nanoparticles for tunable, pH-sensitive and sustained drug release', *Nanoscale* **7**(21), 9497–9504.

Shirakura, T., Smith, C., Hopkins, T. J. J., Lee, Y. E. K., Lazaridis, F., Argyrakis, P. and Kopelman, R. (2017), 'Matrix density engineering of hydrogel nanoparticles with simulation-guided synthesis for tuning drug release and cellular uptake', *ACS Omega* **2**(7), 3380–3389.

Tandon, B., Magaz, A., Balint, R., Blaker, J. J. and Cartmell, S. H. (2018), 'Electroactive biomaterials: Vehicles for controlled delivery of therapeutic agents for drug delivery and tissue regeneration', *Advanced Drug Delivery Reviews* **129**, 148–168.

Tiwari, A. P., Hwang, T. I., Oh, J.-M., Maharjan, B., Chun, S., Kim, B. S., Joshi, M. K., Park, C. H. and Kim, C. S. (2018), 'pH/NIR-responsive polypyrrole-functionalized fibrous localized drug-delivery platform for synergistic cancer therapy', *ACS Applied Materials & Interfaces* **10**(24), 20256–20270.

Uppalapati, D., Boyd, B. J., Garg, S., Travas-Sejdic, J. and Svirskis, D. (2016), 'Conducting polymers with defined micro- or nanostructures for drug delivery', *Biomaterials* **111**, 149–162.

Wallace, G. G., Teasdale, P. R., Spinks, G. M. and Kane-Maguire, L. A. P. (2002), 'Conductive electroactive polymers : Intelligent materials systems, second edition', *Conductive Electroactive Polymers* .

Chapter 5

Biocompatibility of PEGDA-PPy Hydrogels and Application for Cartilage Cell Attachment

This chapter explores the biocompatibility of PEGDA and composite PEGDA-PPy hydrogels. Cytotoxicity testing was performed according to ISO Protocol #10993: *Biological evaluation of medical devices*. Protein adsorption and cell attachment to biomaterials were investigated to explore the potential application of PEGDA-PPy in cartilage tissue engineering.

5.1 Introduction

Every material before placed into contact with biological tissues or cellular environment should meet the biocompatibility requirements. Most importantly, biomaterials should not cause any toxic or immunological reactions in vivo. However, biocompatibility of a material in its broad definition, is not just an absence of cytotoxicity, but also characterises a capacity of a material to interact with in vivo environment (Lotfi et al.,

2013).

Adhesion of cells to the surface of biomaterial is a requirement for cell delivery and tissue regeneration. This is a complex process including the formation of focal adhesion points through cell adhesion proteins (i.e. fibronectin, laminin etc.), cell signaling, and possible alterations of the biomaterial. Biomaterial factors involved in this process are chemical composition, surface roughness, and electric charge (Lotfi et al., 2013). Surface morphology specifically plays an important role as it not just provides a substrate for cell attachment, but also could have a specific effect on cell behaviour (Cai et al., 2020). On rough surfaces, cells form many focal attachment points and the arrangement of cytoskeleton is usually followed by the production of extracellular matrix proteins. This information encoded in protein and gene sequences is passed to other cells, therefore, cell and subsequently tissue phenotype are changed (Boyan et al., 1996). Additionally, surface morphology governs the hydrophilicity and wettability of the material, which are the properties important for protein adhesion (Lotfi et al., 2013).

In biomaterial design, functionalization with factors that promote cell adhesion and proliferation is a vital consideration for a material that is involved in tissue regenerative processes (Bellis, 2011). The indirect functionalization approach involves enhancing protein adsorption to the biomaterial. The direct approach implies grafting of a biomaterial surface with peptides and growth factors stimulating cell adhesion (Mcfarland et al., 2000). Surface morphology modifications have been also explored for promoting cell attachment. Specifically, in the area of metal bone and dental implants, many chemical and mechanical surface modifications were exploited to enhance adhesion of bone cells (Zareidoost et al., 2012).

As previously described in section 2.3.1, PEGDA hydrogels do not provide a supportive environment for cell attachment and need to be modified with bioactive molecules for tissue engineering applications (Choi et al., 2019; Zhu, 2010). PPy as a biocompatible co-polymer in the structure of PEGDA-PPy composite materials, offers many advanta-

geous properties. In the study by He et al. (2017), the typical *cauliflower* appearance of the polymer has been found to be beneficial for the attachment of osteoblastic cell line. In work by Lawrence (2021), PEGDA hydrogels containing PPy NPs demonstrated increased rates of pre-osteoblast cell adhesion, and cells were preferentially adhered to PPy, stretching between the the clusters of NPs.

In section 3.3.3 SEM pictures of PEGDA-PPy hydrogels prepared with interfacial chemical polymerization (ICP) method have demonstrated different surface morphologies compared to PEGDA hydrogels, and between two ICP methods. Therefore, it was hypothesized, that an addition of PPy would allow for protein adsorption and cell attachment to PEGDA, and increased surface roughness of PEGDA-PPy-b materials would enhance the biocompatibility.

5.2 Materials and Methods

5.2.1 Cytotoxicity testing

Cell culture media was prepared by combining Dulbecco's Modified Eagle Medium/Nutrient Mixture F-12 (DMEM/F-12) (ThermoFisher Cat. #11330032), 10 % fetal bovine serum (FBS) (ThermoFisher Cat. #12483020) and 1 % Penicillin-Streptomycin (ThermoFisher Cat. #15140122) followed by sterile filtration. ATDC5 chondrogenic cells derived from mouse teratocarcinoma were used in this experiment (Yao and Wang, 2013).

PEGDA and PEGDA-PPy-a hydrogels were prepared in triplicates. Prior to cytotoxicity testing, samples were thoroughly washed with 70 % ethanol three times and left in ethanol overnight for sterilization. The following day, samples were transferred to the bio-safety cabinet where they were washed twice with Dulbecco's phosphate-buffered saline (DPBS) (ThermoFisher Cat. #14190144) for 10 min, followed by a cell culture media soak for 30 min. Each sample was then moved into an individual well of

a 24-well cell culture plate. The average surface area of each sample in swollen state was determined as 2.7 cm^2 based off the casting molds used. According to the ISO 10993-12: Section 10.3.3, for samples with thickness $\leq$ 1 mm, 1 mL of media is required for a sample with surface area of 3 cm^2. Therefore, 900 µL of full cell culture media was added to each well containing sample. This media specifically contained DMEM/F-12 without phenol red (ThermoFisher Cat. #21041025). Polymers were incubated at 37 ℃ for 14 d, 7 d, 72 h and 24 h. Hydrogel soaking periods were staggered-started so that all media would reach the desired time-point on a single day when the ATDC5 cells reach 80 % confluency.

Two days prior to the end of the hydrogel media soaking period, ATDC5 cells were passaged into 96-well plates with a density 2500 cells/well (passage n=3). Three plates were created where cells at different passages were plated (n=4, 5 or 6) to create three biological replicates. Additionally, two triplicates of the following cell densities: 500 , 1000 , 2500 , 5000 and 7500 cells/well were plated, to build the standard curve through matching the absorbance values from the XTT assay to the cell counts. Standard curves were created separately for each biological replicate. When cells reached 80 % confluency, original cell culture media was replaced with 100 µL of the cell culture conditioned by hydrogel soaking. Negative control wells had 35 µmol of the Sodium Dodecyl Sulfate (SDS, Sigma Aldrich Cat. #151213) solution in culture media. Positive control well contained fresh cell culture media (no phenol red). Three wells were left blank. ATDC5 cells were left to incubate for 24 h.

The next day, the XTT Cell viability assay was performed according to the manufacturer's protocol (ThermoFisher Cat. #X12223). 2 mL of the Electron Coupling Reagent was added to 12 mL of XTT solution and vortexed. The solution was used immediately by adding 70 µL to each test well and one of the standard curve well groups. Plates were left to incubate for 4 h at 37 ℃. Following incubation, the plates were transferred to the TECAN Safire plate reader. Absorbance values were collected at 450 nm for XTT

absorption and at 660 nm for background absorbance. Specific absorbance and cell viability were calculated using the following formula:

$$\text{Absorbance} = \text{Abs}_{450}(\text{Test}) - \text{Abs}_{450}(\text{Blank}) - \text{Abs}_{660}(\text{Test}) \tag{5.1}$$

$$\%\ \text{Viability} = \frac{\text{Abs}_{450}(\text{Test}) - \text{Abs}_{660}(\text{Test})}{\text{Abs}_{450}((+)\ \text{Control}) - \text{Abs}_{660}((+)\ \text{Blank})} \times 100\% \tag{5.2}$$

The second group of standard curve wells was used for cell counts. To each well 30 µL of trypsin (0.25 w/v solution) was added, followed by short incubation (4 min) and neutralization with 70 µL of cell culture media. Cells were counted with a hemocytometer and cell numbers were matched to the XTT absorbance values from the first group of standard curve wells. Prior to performing cell counts, the representative images of ATDC5 cells cultured at 2500/well density were taken with a Leica Phase Contrast Microscope.

Average cell viability and cell count values along with the standard deviations were calculated using the data from 3 biological replicates (3 plates with cells at different passage n), triplicates for each hydrogel type, and 3 technical replicates (total n=27). One-way analysis of variance (ANOVA) and multiple comparison test were performed in MATLAB.

5.2.2 Protein adsorption and cell attachment

To test the adsorption of proteins to hydrogels, PEGDA, PEGDA-PPy-a, and PEGDA-PPy-b were soaked in protein solutions for either 2 h or 24 h in triplicates. The negative control group contained samples soaked in DPBS for 24 h. Two different protein solutions were used: Bovine Serum Albumin (BSA) (ThermoFisher Cat. #0023210) and FBS. At designated time points, samples were rinsed with DPBS to remove any loosely bound proteins, and put in the 1 % SDS solution in DPBS. Samples were placed on a rocker mixer for 2 h to facilitate the elution of proteins in SDS. The Pierce TM Rapid Gold BCA

Protein Assay Kit (ThermoFisher Cat. #A53225) was used to measure the amount of protein adsorbed. 20 µL of the SDS solution from each sample was mixed with 200 µL of the working reagent from the kit. Cu^{+} ion in the working reagent is reduced by the protein in an alkaline media resulting in the orange-gold reaction product. The absorbance of the reaction product was collected using a TECAN Safire Plate Reader at 480 nm, and protein concentrations were calculated using the standard curve obtained with BSA standard solutions. One-way analysis of variance (ANOVA) of the absorbance data and multiple comparison test were performed to in MATLAB.

For a cell attachment study, PEGDA, PEGDA-PPy-a and PEGDA-PPy-b samples were prepared in disc shapes, with a diameter of 15 mm and 1 mm thickness to cover the well in the 24-well plate. Samples were soaked in 70 % ethanol overnight and the next day were transferred into the bio-safety cabinet. Each sample was placed in the individual well of the 24-well plate, washed with DPBS twice for 10 min and then 1 mL of cell culture media was added. Samples were incubated in the media for 2 h in 37 ℃ to facilitate the adsorption of proteins to the surface. The next day, ATDC5 cells were passaged and 200 µL of cell suspension was placed on the sample surface achieving the final plating density of 5000 cells/cm^2. Additionally, cells were plated on to tissue culture plastic at the same density to create a positive control well. Samples with cells were incubated for 1 h at 37 ℃ to allow cells to attach to the surface, and then 800 µL of media was added to achieve the final volume of 1 mL in each well. Samples with cells were left to incubate for 3 d, and then cell fixation was performed. Firstly, cell culture media was aspirated, followed by double rinsing with PBS. Then, 0.5 mL of 4 % (w/v) of polyformaldehyde (PFA) solution was added to each well. After 10 min PFA was removed and samples were washed with PBS again. To visualize the actin fibers of cells, staining with Alexa Fluor 488 Phalloidin was performed (Invitrogen Cat. # A12379). Firstly, blocking solution (1 % BSA in PBS) was applied to cells for 30 min followed by washing with PBS twice for 5 min each. Then, 20 µL of stock Phalloidin

was dissoved in 800 µL of PBS and 100 µL of diluted stain was added to each well and incubated for 20 min at room temperature with agitation. After incubation the stain was removed and wells were washed with PBS. To visualize cell nuclei, Hoechst staining was performed as follows: 0.5 mL of 1 $\mu g \cdot mL^{-1}$ of Hoechst stain (Sigma Aldrich Cat. #33342) was added to each well and the plate was kept on a rocker mixer for 20 min at room temperature, protected from light. After staining, Hoechst solution was removed, samples were washed with PBS twice for 10 min, then fresh PBS was added to each well to keep samples hydrated during imaging. Cells were imaged with a Leica DMI6000 microscope.

5.3 Results and Discussion

5.3.1 Cytotoxicity testing

The results of the biocompatibility testing for PEGDA hydrogels and PEGDA-PPy conducting hydrogels are summarized in fig. 5.1 and table 5.1. Positive control wells where cells were cultured in fresh media, were taken as 100 % viability. Figure 5.2 (a) is a phase contrast image of healthy ATDC5 culture from the positive control well. The ISO Protocol #10993: *Biological evaluation of medical devices* defines cytotoxicity as $\leq$ 70 % cell viability (ISO 10993-1:2018, 2018). Cytotoxic effects of SDS solution can be clearly seen in the negative control wells, where cells only demonstrated 22 % viability. A representative phase contrast image of the cell culture well treated with SDS is shown in fig. 5.2 (b).

Overall, media extracts from PEGDA and PEGDA-PPy samples did not show any cytotoxic effect on ATDC5 cells. Average cell viability for PEGDA-PPy samples ranged from 77 % (24 h) to 137 % (7 d). A decrease in cell viability for a short time-point was not significantly different from the positive control, and was higher than 70 % viability level that indicates cytotoxicity. Possible sources of cytotoxicity are solvents and uncured

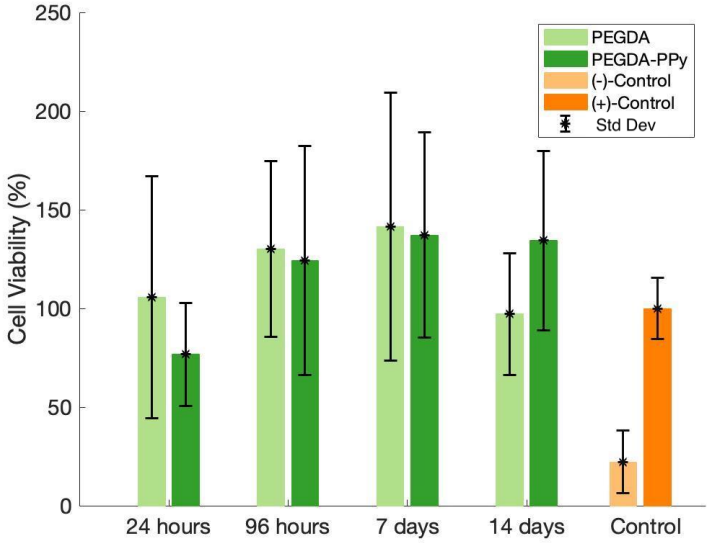

Figure 5.1: Viability of ATDC5 cells treated with media extracts from PEGDA and PEGDA-PPy hydrogels calculated from XTT assay using the eq. (5.2). Average viability (%) is plotted with the standard deviation. Total n of data points used = 27 = (3 technical replicates X 3 of each hydrogel type) X 3 biological repetitions of the test with cells at different passages. There was no significant difference between sample groups and time-points compared to the positive control (100 %), indicating no cytotoxic effect.

monomers entrapped in polymer network which should be effectively washed out from PEGDA-PPy with ethanol. A slight decrease in cell viability for a short time media soak could indicate an insufficient washing, however, the viability levels did not indicate any cytotoxicity. Importantly, due to the non-degradable nature of PEGDA-PPy materials, longer time-points for polymer media soak were introduced in this biocompatibility study. It can be clearly seen in fig. 5.1 that cell viability slightly increased for longer polymer exposure times.

Average cell viability for PEGDA hydrogels was not significantly different from PEGDA-PPy, and was ranging from 97 % (14 d) to 141 % (7 d). A major concern for the biocompatibility of PEGDA hydrogels comes from the possible toxic effects of PI used for cross-linking and free radicals generated during the polymerization reaction. The PI used for PEGDA polymerization in this study, LAP, is cytocompatible (Choi et al., 2019).

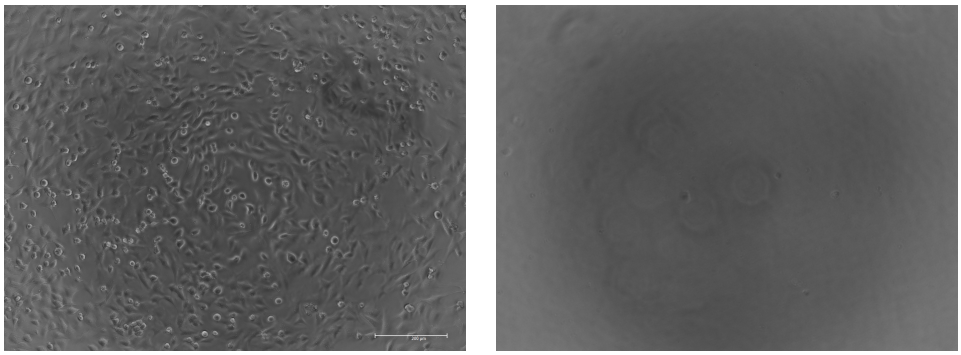

(a) (b)

Figure 5.2: Phase contrast images taken at 10× magnification of positive control well from XTT viability study representing healthy ATDC5 cell culture plated at 2500 cells/well (a), and negative control well representing dead cells treated with SDS solution (b). Scale bar represents 200 µm.

Cell Counts (Mean ±Standard Deviation)				
Sample	24 h	72 h	7 d	14 d
PEGDA-PPy	4 934±4 445	10 985±10 033	11 712±8 486	11 364±7 975
PEGDA	9 370±10 271	10 901±7 450	12 894±11 882	7 160±5 533

Table 5.1: Calculated cells/well from the XTT specific absorbance data using the plated standard curves to create a linear formula relating absorbance to cell numbers. No statistical difference was seen between any time-points or types of samples. Results are reported with the standard deviation. Total n of data points used = 27 = (3 technical replicates X 3 of each hydrogel type) X 3 biological repetitions of the test with cells at different passages. Mean values were rounded to the nearest hundredth.

In the study performed by Fairbanks et al. (2009) 96 % survival rate was reported for fibroblasts encapsulated in PEGDA hydrogels photo polymerized using the LAP initiator. The results of the XTT study confirm the absence of any cytotoxic effect in the media extracts taken from PEGDA hydrogels.

5.3.2 Protein adsorption and cell attachment

Proteins adsorbed to the surfaces of PEGDA, or PEGDA-PPy hydrogels can be extracted from samples following SDS detergent treatment and detected using the BCA Protein

Assay kit. Figure 5.3 demonstrates no significant difference between absorbance values of the extract solutions from experimental samples and negative control group samples. There is also no significant difference in absorbance values between the two different types of proteins used (FBS or BSA) or in the duration of exposure of samples to protein solutions. Given the similar absorbance values of solutions that do not contain protein (negative control group) and solutions expected to contain protein (experimental sample group), it was concluded that no protein was extracted from hydrogel samples. Therefore, absorbance values have not been converted into protein concentrations.

Protein adsorption to the surface of TE scaffolds is an important step preceding cell attachment (Moroder et al., 2011). PEGDA hydrogels as PEG derivatives are intrinsically resistant to protein adsorption and, therefore, do not support cell attachment (Choi et al., 2019). PPy, on the other hand, has been utilized as a substrate for cell attachment in numerous studies, as described in section 2.2.3. Schmidt et al. (1997) demonstrated improved interactions of PC-12 cells with PPy films. This study described enhanced cell attachment as a result of increased adsorption of positively-charged proteins to the negatively charged surface of PPy films. In the study by Moroder et al. (2011), polycaprolactone fumarate-PPy scaffolds have demonstrated the adsorption of proteins and nerve growth factor from the media. However, it is important to mention, that in both studies PPy has been doped with large anionic dopant: poly(styrenesulfonate) (Schmidt et al., 1997), naphthalene sulfonic acid (NSA) or dodecylbenzene sulfonic acid (DBSA) (Moroder et al., 2011), which according to Schmidt et al. (1997) are responsible for the high surface negative charge of materials.

PEGDA-PPy hydrogels used for the protein adsorption study in this thesis did not contain any dopants, except for the persulfate ion coming from the APS oxidizer during polymerization. The absence of large anionic dopants may have been a potential drawback which can be addressed in future studies.

Differences in surface morphology between PEGDA-PPy-a and PEGDA-PPy-b

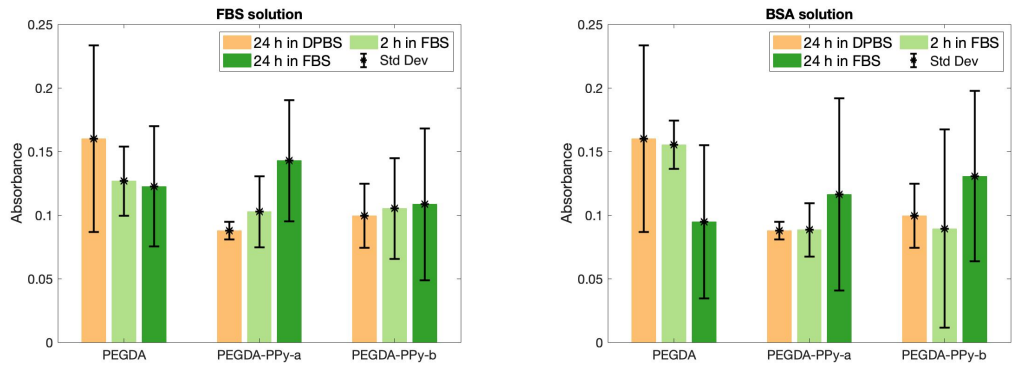

(a) (b)

Figure 5.3: Mean absorbance values ($\pm$ standard deviation) of SDS solutions used for the extraction of FBS (a) BSA (b) proteins from PEGDA, PEGDA-PPy-a, and PEGDA-PPy samples immersed in protein solutions for 2 h or 24 h. No significant difference was observed in absorbance values between samples and negative control group representing materials immersed in DPBS, indicating the absence of protein in SDS extracts.

have been hypothesized to influence the adhesion of proteins and, subsequently, cell attachment. However, as mentioned earlier, no proteins were detected in extract solutions from either of samples. Additionally, it is possible that the conditions of SDS solution treatment were insufficient to lift proteins from sample surfaces. Park and Bae (2002) investigated the properties of poly(ethylene oxide) (PEO) and poly(tetramethylene oxide) (PTMO) copolymer coatings for use in hemocompatible devices where protein adsorption to materials is undesirable. In this study, for the detection of proteins adsorbed to PEO/PTMO, samples were submerged in BSA, followed by sonication in 1 % SDS solution for 30 min to achieve maximum SDS-protein binding. It is likely that sonication may be required to facilitate the detachment of proteins from PEGDA-PPy hydrogels as well.

Fluorescent images of positive control well, PEGDA and PEGDA-PPy hydrogels with fixated cells collected at low magnifications (5×) are presented on fig. 5.4. Nuclei of ATDC5 cells can be clearly visualized on PEGDA-PPy-a samples (fig. 5.4 (a)). It can also be seen that cells are organized in clusters of two or three. The amount of cells

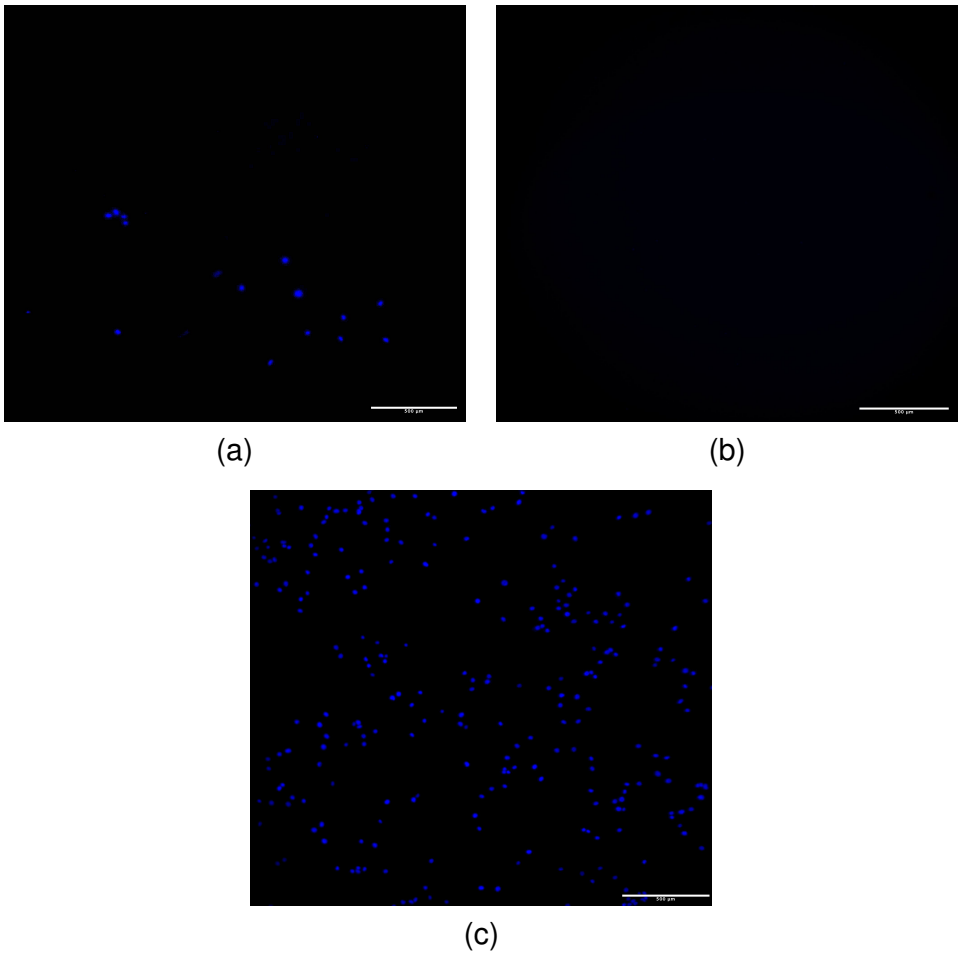

(a) (b)

(c)

Figure 5.4: Fluorescent images of Hoechst stained PEGDA-PPy-a (a), PEGDA hydrogels (b) and TCP (c). ATDC5 cell nuclei can be visualized on the surface of PEGDA-PPy-a materials and tissue culture plastic indicating successful cell attachment. Scale bar represents 500 µm.

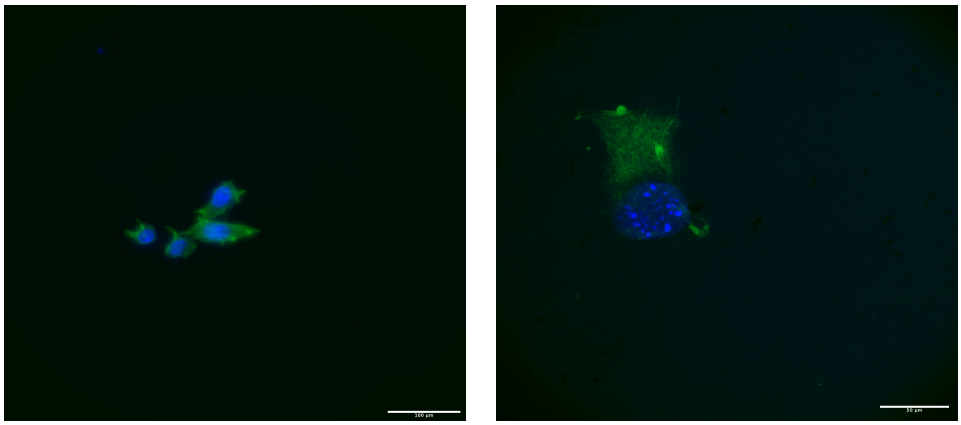

(a) (b)

Figure 5.5: Hoechst and phalloidin stained ATDC5 cells adhered to PEGDA-PPy-a (a). Actin fibers stained with phalloidin (green) are extended from the centre of the cell with nucleus (stained blue) indicating the formation of attachment points on the material. Scale bar represents 100 µm (a) and 50 µm (b).

attached to PEGDA-PPy-a samples is significantly lower than number of cells adhered to tissue culture plastic (fig. 5.4 (c)). As expected, no cells were attached to the surface of PEGDA hydrogel (fig. 5.4 (b)). Interestingly, PEGDA-PPy-b hydrogels have also demonstrated no cell attachment. The morphology of cells attached to PEGDA-PPy-a and stained with both the nuclear Hoechst stain and phalloidin actin stain is presented on fig. 5.5. It can be clearly seen that cells have several attachment points, however, actin fibers are mostly concentrated around the nuclei.

An addition of PPy to PEGDA hydrogel has led to the successful attachment of ATDC5 cells to the material. As described in section 2.2.3, PPy has been investigated as a substrate for cell adhesion and overall has demonstrated high attachment rates for cardiac progenitor cells (Gelmi et al., 2014), osteoblasts (Giglio et al., 2000*a*), and human fibroblasts (Moreno et al., 2008). An improvement of pre-osteoblast cell attachment to PEGDA hydrogels was previously achieved through the addition of PPy nanoparticles in the work by Lawrence (2021). This thesis is a first study describing successful adhesion of cartilagenious ATDC5 cells to PEGDA-PPy hydrogels.

The absence of cell adhesion on PEGDA-PPy-b could be a result of the increased surface roughness of the material as opposed to the initial hypothesis. In general, material roughness at micro- and nanoscale are considered to be the most successful in promoting cell adhesion and growth (Cai et al., 2020; He et al., 2017). In the study done by Kay et al. (2004), improved osteoblast and chondrocyte adhesion was seen on PLGA film surfaces with nanometer roughness dimensions compared to micron dimensions. It is likely that the roughness of PEGDA-PPy-b did not support cell attachment. Additionally, as discussed in section 3.3.3, surface morphology has a direct impact on surface free energy and wettability. These parameters also affect adsorption of proteins and help to stabilize the formed protein complexes (Lotfi et al., 2013). Future studies could investigate contact angle and hydrophilicity parameters of PEGDA-PPy-a and PEGDA-PPy-b hydrogels.

Direct functionalization of PEGDA-PPy materials with cell adhesion peptides or other proteins is also a promising method to enhance cell attachment and proliferation on scaffolds. For example, the amino acid sequence arginine-glycine-aspartate also known as RGD-peptide which is naturally present in the structure of ECM poteins, have been extensively investigated for grafting of biomaterials (Bellis, 2011). Electrochemically deposited PPy films have been previously doped with RGD peptide in studies by Giglio et al. (2000*b*); Li and Yu (2017), and have demonstrated significantly higher levels of osteoblast cell attachment than to non-modified films (Giglio et al., 2000*b*). Future studies can investigate grafting of PEGDA-PPy with RGD peptide through the doping during chemical polymerization. An improved electrochemical performance of PEGDA-PPy-b described in section 3.3.2 should also allow for electrochemical doping and can ensure higher drug loading.

5.4 Chapter summary

This chapter described the biocompatibility testing of PEGDA hydrogels and PEGDA-PPy composite materials. Both types of materials demonstrated the absence of any cytotoxic effect on ATDC5 cells over the 14 d period. The absence of cytotoxicity confirms the safety of photo-crosslinking and interfacial chemical polymerization methods used for material fabrication. Although, protein adsorption study did not yield any positive results, successful attachment of ATDC5 cells to PEGDA-PPy was demonstrated. Future studies could focus on qualitative characterization of the attached cells. Modifications of PEGDA-PPy such as PPy doping with anionic compounds or peptides could be explored as a method to facilitate protein adsorption and cell adhesion.

5.5 List of references

Bellis, S. L. (2011), 'Advantages of RGD peptides for directing cell association with biomaterials', *Biomaterials* **32**(18), 4205–4210.

Boyan, B. D., Hummert, T. W., Dean, D. D. and Schwartz, Z. (1996), 'Role of material surfaces in regulating bone and cartilage cell response', *Biomaterials* **17**(2), 137–146.

Cai, S., Wu, C., Yang, W., Liang, W., Yu, H. and Liu, L. (2020), 'Recent advance in surface modification for regulating cell adhesion and behaviors', *Nanotechnology Reviews* **9**(1), 971–989.

Choi, J. R., Yong, K. W., Choi, J. Y. and Cowie, A. C. (2019), 'Recent advances in photo-crosslinkable hydrogels for biomedical applications', *BioTechniques* **66**(1), 40–53.

Fairbanks, B. D., Schwartz, M. P., Bowman, C. N. and Anseth, K. S. (2009), 'Photoinitiated polymerization of PEG-diacrylate with lithium phenyl-2,4,6-

trimethylbenzoylphosphinate: polymerization rate and cytocompatibility', *Biomaterials* **30**(35), 6702–6707.

Gelmi, A., Ljunggren, M. K., Rafat, M. and Jager, E. W. (2014), 'Influence of conductive polymer doping on the viability of cardiac progenitor cells', *Journal of Materials Chemistry B* **2**(24), 3860–3867.

Giglio, E. D., Sabbatini, L., Colucci, S. and Zambonin, G. (2000*a*), 'Synthesis, analytical characterization, and osteoblast adhesion properties on RGD-grafted polypyrrole coatings on titanium substrates', *Journal of Biomaterials Science, Polymer Edition* **11**(10), 1073–1083.

Giglio, E. D., Sabbatini, L., Colucci, S. and Zambonin, G. (2000*b*), 'Synthesis, analytical characterization, and osteoblast adhesion properties on RGD-grafted polypyrrole coatings on titanium substrates', *Journal of Biomaterials Science, Polymer Edition* **11**(10), 1073–1083.

He, Y., Wang, S., Mu, J., Dai, L., Zhang, Z., Sun, Y., Shi, W. and Ge, D. (2017), 'Synthesis of polypyrrole nanowires with positive effect on mc3t3-e1 cell functions through electrical stimulation', *Materials Science and Engineering: C* **71**, 43–50.

ISO 10993-1:2018 (2018), Biological evaluation of medical devices — Part 1: Evaluation and testing within a risk management process, Standard, International Organization for Standardization, Geneva, CH.

Kay, S., Thapa, A., Haberstroh, K. M. and Webster, T. J. (2004), 'Nanostructured polymer/nanophase ceramic composites enhance osteoblast and chondrocyte adhesion', *https://home.liebertpub.com/ten* **8**(5), 753–761.

Lawrence, M. (2021), '3D printed polypyrrole scaffolds for pH dependent drug delivery with applications in bone regeneration', *The University of Western Ontario Electronic Thesis and Dissertation Repository* **7837**.

Li, Y. and Yu, C. (2017), 'RGD peptide doped polypyrrole film as a biomimetic electrode coating for impedimetric sensing of cell proliferation and cytotoxicity', *Journal of Applied Biomedicine* **15**(4), 256–264.

Lotfi, M., Nejib, M. and Naceur, M. (2013), 'Cell adhesion to biomaterials: Concept of biocompatibility', *Advances in Biomaterials Science and Biomedical Applications* .

Mcfarland, C. D., Thomas, C. H., Defilippis, C., Steele, J. G. and Healy, K. E. (2000), 'Protein adsorption and cell attachment to patterned surfaces'.

Moreno, J. S., Panero, S., Artico, M. and Filippini, P. (2008), 'Synthesis and characterization of new electroactive polypyrrole-chondroitin sulphate a substrates', *Bioelectrochemistry* **72**(1), 3–9.

Moroder, P., Runge, M. B., Wang, H., Ruesink, T., Lu, L., Spinner, R. J., Windebank, A. J. and Yaszemski, M. J. (2011), 'Material properties and electrical stimulation regimens of polycaprolactone fumarate-polypyrrole scaffolds as potential conductive nerve conduits', *Acta Biomaterialia* **7**(3), 944–953.

Park, J. H. and Bae, Y. H. (2002), 'Physicochemical properties and in vitro biocompatibility of peo/ptmo multiblock copolymer/segmented polyurethane blends', *Journal of biomaterials science. Polymer edition* **13**(5), 527–542.

Schmidt, C. E., Shastri, V. R., Vacanti, J. P. and Langer, R. (1997), 'Stimulation of neurite outgrowth using an electrically conducting polymer', *Proceedings of the National Academy of Sciences of the United States of America* **94**(17), 8948–8953.

Yao, Y. and Wang, Y. (2013), 'ATDC5: An excellent in vitro model cell line for skeletal development', *Journal of Cellular Biochemistry* **114**(6), 1223–1229.

Zareidoost, A., Yousefpour, M., Ghasemi, B. and Amanzadeh, A. (2012), 'The rela-

tionship of surface roughness and cell response of chemical surface modification of titanium', *Journal of Materials Science. Materials in Medicine* **23**(6), 1479.

Zhu, J. (2010), 'Bioactive modification of poly(ethylene glycol) hydrogels for tissue engineering', *Biomaterials* **31**(17), 4639–4656.

Chapter 6

Concluding remarks

6.1 Summary of conclusions

This thesis explored the fabrication of composite PEGDA-PPy hydrogel biomaterials for regenerative cartilage applications. The knowledge ascertained through these studies has prompted the following conclusions:

1. PPy can be successfully incorporated into hydrogels using the interfacial chemical polymerization method. PEGDA hydrogel can serve as PPy deposition matrix, and its physical and mechanical properties, and ultimately the properties of the composite material, can be controlled through varying degrees of hydrogel cross-linking during the photopolymerization of PEGDA. PPy incorporation does not affect the permeability of the hydrogel, moreover, PEGDA-PPy conducting composites demonstrated the capacity for oxidation/reduction reactions. Novel ICP methods was developed to enhance the electrochemical performance and create distinctive surface morphology.

2. A PEGDA resin formulation was developed for the use in the OMASML stereolithography printer, and was successfully applied for the fabrication of porous structures. It was shown that ICP methods can be used to incorporate PPy into 3D

printed structures to create tissue engineering scaffolds with enhanced bioactivity due to the addition of PPy.

3. PPy can be successfully doped with anionic molecules during the chemical oxidative polymerization while being deposited on to PEGDA hydrogel matrix. pH-dependant drug release from PEGDA-PPy material was demonstrated. Drugs incorporated with the composites can be released in solutions at physiologically relevant pH values. PEGDA hydrogels provide an additional level of control over the drug release by slowing down the diffusion of the drug.

4. Finally, biological testing of PEGDA-PPy demonstrated the absence of cytotoxic effect from the material extracts, and indicated improved cell adhesion of ATDC5 cartilaginous cells onto the material surface compared to PEGDA hydrogels alone.

6.2 Summary of contributions

The most significant research contributions presented in this thesis are summarized as follows:

- The first-ever study that introduces a customization of interfacial chemical polymerization as a method to improve electrochemical properties and modify surface morphology of PEGDA-PPy hydrogels for biomedical applications.

- A novel study on the properties and printing parameters of PEGDA resin for stereolithography. Developed resin formulation was applied to fabricate porous lattice structures that serve as a basis for tissue engineering scaffold models. ICP methods were applied to 3D printed porous structure to fabricate PEGDA-PPy electroactive scaffold with resolutions relevant for tissue engineering applications.

- The first to our knowledge study to explore the doping capability of PPy via chemical oxidative polymerization. Novel research on pH-dependant drug release

from PEGDA-PPy demonstrated a contribution of PEGDA hydrogel matrix to the drug release rates in alkaline solutions.

- The first study to explore the biocompatibility of PEGDA-PPy materials with cartilaginous cells ATDC5. Biological study results demonstrated no cytotoxicity and indicated cell adhesion onto the surface of conducting hydrogels. A novel approach to surface modification for PEGDA-PPy hydrogels during chemical polymerization for the improvement of cell attachment has been introduced.

6.3 Recommendations for future research

This thesis is a thorough study on ICP as a method for the drug doping of PPy and its incorporation into the hydrogel matrix. The modification to this method introduced in Chapter 3 led to the fabrication of PEGDA-PPy samples with significantly different electrochemical properties and surface morphologies. Further investigation is needed to expand the knowledge about the conductivity, drug doping and delivery properties of these materials. Contact angle and wettability measurements would help to predict and explain protein and cell adhesion onto surfaces. Additionally, achieving good control over the amount of PPy deposited on the surface could help to further modify surface morphology of PEGDA-PPy materials and obtain optimal parameters for cell attachment.

Developed PEGDA resin formulation has been successful for applications in 3D printing of lattice structures with subsequent PPy deposition for the creation of electroactive tissue engineering scaffolds. Further tuning of the formulation would be to increase the PEGDA concentration to improve the stiffness for the printing of smaller scale features.

Drug release studies demonstrated the ability of PPy in PEGDA-PPy composites to be doped with anionic compounds. Future studies could investigate of doping of PPy with cationic molecules. Due to the capacity of PEGDA-PPy materials for oxidation and reduction under the action of electic potential, reported in this thesis, doping in an

electrochemical cell could be possible to achieve higher rates of drug loading. Testing dopant release over a pH range commonly found in the human body, as well the application of other in vivo relevant release stimuli should be explored.

The expansion to the cell attachment study is needed to investigate the interactions between cells and material surface. Gene expression testing could be done to the cells adhered onto the material and stimulated into cartilaginous differentiation. This would help to understand if the material supports cell activities such as protein synthesis vital for the formation of the new tissue.

Appendices

Appendix A

Copyright Permissions

The following pages provide confirmation of acquired copyright permissions for the appropriate referenced figures in this thesis. Table A.1 summarizes the copyright information, followed by excerpts of the relevant documentation. Permissions are presented in the order they appear in the thesis. Note that copyright permission marked with N/A were either given without a License Number or covered under a Creative Commons license (CCBY).

Table A.1: Summary of copyright permission information

Thesis Figure	Reference Title	Reference Figure	First Author	Publication	Publisher	License Number
2.1	Altered Mechanics of cartilage with osteoarthritis: human osteoarthritis and an experimantal model of joint degeneration	Figure 1	Lori A.Setton	Osteoarthritis and Cartilage	Elsevier	5360240246305
2.2	Progress in preparation, processing and applications of polyaniline	Figure 1	Sambhu Bhadra	Progress in Polymer Science	Elsevier	5360271291782
2.3	Interaction of conducting polymers, polyaniline and polypyrroe, with organic dyes: polymer morphology control, dye adsorption and photocatalytic decomposition	Figure 1	Jaroslav Stejskal	Chemical Papers	Springer Nature	5359700329932
2.4	Electrochemically controlled drug delivery based on intrinsically conducting polymers	Figure 1	Darren Svirskis	Journal of Controlled Release	Elseiver	5360300629273
2.5	Rapid fabrication of hydrogel microstructures using UV-induced projection printing	Figure 5	W. Yang	Micromachines	MDPI	N/A
3.1	Digital light processing for the fabrication of 3D intrinsically conductive polymer structures	Figure 2	Andrew T. Cullen	Synthetic Metals	Elseiver	5360231096338
3.2	A brief description of cyclic voltammetry transducer-based non-enzymatic glucose biosensor using synthesized graphene electrodes	Figure 5	Mohamed Husein Fahmy Taha	Applied System Innovation	MDPI	N/A
3.4 (b)	Influence of conductive polymer doping on theviability of cardiac progenitor cells	Figure 1	A. Gelmi	Journal of Material Chemistry B	Royal Society of Chemistry	N/A
4.1	Fluorescein Derivatives as Fluorescent Probes for pHMonitoring along Recent Biological Applications	Figure 4	Florent Le Guern	International Journal of Molecular Sciences	MDPI	N/A

License Number	5360240246305
License date	Aug 01, 2022

Licensed Content

Licensed Content Publisher	Elsevier
Licensed Content Publication	Osteoarthritis and Cartilage
Licensed Content Title	Altered mechanics of cartilage with osteoarthritis: human osteoarthritis and an experimental model of joint degeneration
Licensed Content Author	Lori A. Setton,Dawn M. Elliott,Van C. Mow
Licensed Content Date	Jan 1, 1999
Licensed Content Volume	7
Licensed Content Issue	1
Licensed Content Pages	13

Order Details

Type of Use	reuse in a thesis/dissertation
Portion	figures/tables/illustrations
Number of figures/tables/illustrations	1
Format	electronic
Are you the author of this Elsevier article?	No
Will you be translating?	No

About Your Work

Title	Conducting polypyrrole hydrogel biomaterials for applications in drug delivery and cartilage tissue regeneration
Institution name	Western University
Expected presentation date	Aug 2022

Additional Data

Portions	Fig.1

Figure A.1: Copyright permission for Figure 2.1

License Number	5360271291782
License date	Aug 01, 2022

Licensed Content

Licensed Content Publisher	Elsevier
Licensed Content Publication	Progress in Polymer Science
Licensed Content Title	Progress in preparation, processing and applications of polyaniline
Licensed Content Author	Sambhu Bhadra,Dipak Khastgir,Nikhil K. Singha,Joong Hee Lee
Licensed Content Date	Aug 1, 2009
Licensed Content Volume	34
Licensed Content Issue	8
Licensed Content Pages	28

Order Details

Type of Use	reuse in a thesis/dissertation
Portion	figures/tables/illustrations
Number of figures/tables/illustrations	1
Format	electronic
Are you the author of this Elsevier article?	No
Will you be translating?	No

About Your Work

Title	Conducting polypyrrole hydrogel biomaterials for applications in drug delivery and cartilage tissue regeneration
Institution name	Western University
Expected presentation date	Aug 2022

Additional Data

Portions	Fig.1

Figure A.2: Copyright permission for Figure 2.2

Your confirmation email will contain your order number for future reference.

License Number	5359700329932
License date	Jul 31, 2022

Printable Details

Licensed Content

Licensed Content Publisher	Springer Nature
Licensed Content Publication	Chemical Papers
Licensed Content Title	Interaction of conducting polymers, polyaniline and polypyrrole, with organic dyes: polymer morphology control, dye adsorption and photocatalytic decomposition
Licensed Content Author	Jaroslav Stejskal
Licensed Content Date	Nov 16, 2019

Order Details

Type of Use	Thesis/Dissertation
Requestor type	non-commercial (non-profit)
Format	electronic
Portion	figures/tables/illustrations
Number of figures/tables/illustrations	1
Will you be translating?	no
Circulation/distribution	200 - 499
Author of this Springer Nature content	no

About Your Work

Title	Conducting polypyrrole hydrogel biomaterials for applications in drug delivery and cartilage tissue regeneration
Institution name	Western University
Expected presentation date	Aug 2022

Additional Data

Portions	Fig.1

Figure A.3: Copyright permission for Figure 2.3

License Number	5360300629273
License date	Aug 01, 2022

Licensed Content

Licensed Content Publisher	Elsevier
Licensed Content Publication	Journal of Controlled Release
Licensed Content Title	Electrochemically controlled drug delivery based on intrinsically conducting polymers
Licensed Content Author	Darren Svirskis,Jadranka Travas-Sejdic,Anthony Rodgers,Sanjay Garg
Licensed Content Date	Aug 17, 2010
Licensed Content Volume	146
Licensed Content Issue	1
Licensed Content Pages	10

Order Details

Type of Use	reuse in a thesis/dissertation
Portion	figures/tables/illustrations
Number of figures/tables/illustrations	1
Format	electronic
Are you the author of this Elsevier article?	No
Will you be translating?	No

About Your Work

Title	Conducting polypyrrole hydrogel biomaterials for applications in drug delivery and cartilage tissue regeneration
Institution name	Western University
Expected presentation date	Aug 2022

Additional Data

Portions	Fig.1

Figure A.4: Copyright permission for Figure 2.4

ELSEVIER LICENSE
TERMS AND CONDITIONS

Aug 02, 2022

This Agreement between Miss. Iryna Liubchak ("You") and Elsevier ("Elsevier") consists of your license details and the terms and conditions provided by Elsevier and Copyright Clearance Center.

License Number	5360231096338
License date	Aug 01, 2022
Licensed Content Publisher	Elsevier
Licensed Content Publication	Synthetic Metals
Licensed Content Title	Digital light processing for the fabrication of 3D intrinsically conductive polymer structures
Licensed Content Author	Andrew T. Cullen,Aaron D. Price
Licensed Content Date	Jan 1, 2018
Licensed Content Volume	235
Licensed Content Issue	n/a
Licensed Content Pages	8
Start Page	34
End Page	41
Type of Use	reuse in a thesis/dissertation
Portion	figures/tables/illustrations

Figure A.5: Copyright permission for Figure 3.1

Influence of conductive polymer doping on the viability of cardiac progenitor cells

A. Gelmi, M. K. Ljunggren, M. Rafat and E. W. H. Jager, *J. Mater. Chem. B*, 2014, **2**, 3860 **DOI:** 10.1039/C4TB00142G

Figure A.6: Copyright permission for Figure 3.4 (b)

Curriculum Vitæ

Name:	Iryna Liubchak
Post-Secondary Education and Degrees:	Sumy State University Sumy, Ukraine 2014 – 2020 M.D.
Honours and Awards:	Ontario Graduate Scholarship 2021 – 2022 Western's Collaborative Training Program in MSK Health Research Transdisciplinary Training Award 2020 – 2021 Mitacs Globalink Graduate Fellowship 2020 – 2021
Related Work Experience:	Teaching Assistant The University of Western Ontario Biology 1002B: Biology for Sciences II 2022

Publications:

Liubchak, I., Lawrence, M. T., Holness, F. B. and Price, A. D. (2020), 'Soft template electropolymerization of polypyrrole for improved pH-induced drug delivery', *International Journal of Molecular Sciences* **21**(21), 8114.

Liubchak, I., Lawrence, M. T., Holness, F. B. and Price, A. D. (2021), Soft-template electrochemical polymerization for the advancement of electroactive polymer drug delivery systems, *in* 'Electroactive Polymer Actuators and Devices (EAPAD) XXIII', Vol. 11587, International Society for Optics and Photonics, SPIE, pp. 103 – 109.